The Meteoritical Society

Meteoritics & Planetary Science 44, Nr 5, 725–745 (2009)
Abstract available online at http://meteoritics.org

Expanding the application of the Eu-oxybarometer to the lherzolitic shergottites and nakhlites: Implications for the oxidation state heterogeneity of the Martian interior

Molly C. McCANTA[1, 4*], Linda ELKINS-TANTON[2], and Malcolm J. RUTHERFORD[3]

[1]California Institute of Technology, Department of Geological and Planetary Sciences, MS 170-25, Pasadena, California 91125, USA
[2]Massachusetts Institute of Technology, Department of Earth, Atmospheric, and Planetary Sciences, 77 Massachusetts Ave., Building 54, Room 824, Cambridge, Massachusetts 02139, USA
[3]Brown University, Department of Geological Sciences, 324 Brook St., Providence, Rhode Island 02912, USA
[4]Present address: Tufts University, Geology Department, Lane Hall, 2 North Hill Road, Medford, Massachusetts 02155, USA
[*]Corresponding author. E-mail: molly.mccanta@tufts.edu

(Received 07 July 2008; revision accepted 06 February 2009)

Abstract–Experimentally rehomogenized melt inclusions from the nakhlite Miller Range 03346 (MIL 03346) and the lherzolitic shergottite Allan Hills 77005 (ALH 77005) have been analyzed for their rare earth element (REE) concentrations in order to characterize the early melt compositions of these Martian meteorites and to calculate the oxygen fugacity conditions they crystallized under. $D(Eu/Sm)_{pyroxene/melt}$ values were measured at 0.77 and 1.05 for ALH 77005 and MIL 03346, respectively. These melts and their associated whole rock compositions have similar REE patterns, suggesting that whole rock REE values are representative of those of the early melts and can be used as input into the pyroxene Eu-oxybarometer for the nakhlites and lherzolitic shergottites. Crystallization fO_2 values of IW + 1.1 (ALH 77005) and IW + 3.2 (MIL 03346) were calculated. Whole rock data from other nakhlites and lherzolitic shergottites was input into the Eu-oxybarometer to determine their crystallization fO_2 values. The lherzolitic shergottites and nakhlites have fO_2 values that range from IW + 0.4 to 1.6 and from IW + 1.1 to 3.2, respectively. These values are consistent with some previously determined fO_2 estimates and expand the known range of fO_2 values of the Martian interior to four orders of magnitude. The origins of this range are not well constrained. Possible mechanisms for producing this spread in fO_2 values include mineral/melt fractionation, assimilation, shock effects, and magma ocean crystallization processes. Mineral/melt partitioning can result in changes in fO_2 from the start to the finish of crystallization of 2 orders of magnitude. In addition, crystallization of a Martian magma ocean with reasonable initial water content results in oxidized, water-rich, late-stage cumulates. Sampling of these oxidized cumulates or interactions between reduced melts and the oxidized material can potentially account for the range of fO_2 values observed in the Martian meteorites.

INTRODUCTION

An understanding of the interior oxygen fugacity (fO_2) of a planet is vital for modeling its formation and evolution. During accretion, the ability to retain elements such as C and S in a growing planetary body depends in part on the oxidation state (and temperature) of the material in the accretion zone (Righter and Drake 1996; Li and Agee 2001; Chabot and Agee 2003). Additionally, numerous studies illustrate that the partitioning of siderophile elements, such as W, Pt, and Ni, between the proto-core and mantle during differentiation is also dependent on the fO_2 of the system (e.g., Brett 1984; Palme and O'Neill 1996; O'Neill 2004; Cottrell and Walker 2006). Finally, the partitioning of many elements between melt and the residuum during partial mantle melting is dependent on fO_2 (O'Neill and Wall 1987). Therefore, knowledge of the fO_2 systematics of a planetary body is necessary when reconstructing its evolutionary history.

Measurements of the fO_2 of an igneous system can be made using a variety of oxybarometers which rely on multivalent element partitioning. Examples of these oxybarometers include: the Fe^{2+}/Fe^{3+} ratios of oxides or silicate melts; mineral equilibria, such as olivine-pyroxene-spinel; and ratios of other multivalent elements including Eu, Cr, and V (Buddington and Lindsley 1964; Sack et al. 1980; Ballhaus et al. 1990; Kress and Carmichael 1991; Wood 1991;

McKay et al. 1994; Wadhwa 2001; McCanta et al. 2004; Karner et al. 2006; Shearer et al. 2006; Karner et al. 2007a, 2007b). On Earth, the fO_2 of magmas reaching the planet's surface is known to range over nine orders of magnitude (Carmichael 1991; Parkinson and Arculus 1999). This range is potentially the result of one or more factors, including primary source region differences, melt dehydrogenation or other volatile loss, water or melt infiltration, assimilation of oxidized or reduced wallrock, closed system mineral/melt partitioning, and reintroduction of altered material into the mantle and subsequent mixing due to subduction and convection (Brandon and Draper 1996; Amundsen and Neumann 1992; Ague 1998; Frost and Ballhaus 1998; Parkinson and Arculus 1999).

Few meteorite groups in the current meteorite collection exhibit any significant range in fO_2 within the group or show any evidence of oxidized material. The fO_2 of lunar magmas is low and relatively constant at iron-wüstite (IW–0.5 ± 1.0) as indicated by the fairly ubiquitous presence of Fe-rich metal (Sato et al. 1973; Usselman and Lofgren 1976; Haggerty 1978; Sato 1978; Nicholis and Rutherford 2005). With the notable exception of the Martian meteorites, the R chondrites (Nakamura et al. 1993; Bischoff et al. 1994; Rubin and Kallemeyn 1994; Schulze et al. 1994; Kallemeyn et al. 1996), and some carbonaceous chondrite groups (e.g., Larimer and Wasson 1988; Brearley and Jones 1998), most meteorite parent bodies also have compositional characteristics (Fe-metal phases) requiring they crystallized at fO_2 values of IW or below (e.g., eucrites: Stolper 1977, acapulcoites and lodranites: Benedix and Lauretta 2006, ureilites: Walker and Grove 1993).

Based on a variety of analytical methods, the basaltic shergottites, a class of meteorites from Mars, exhibit a range of intrinsic fO_2 values spanning 2–3 orders of magnitude including several meteorites that indicate they were crystallized under fairly oxidizing conditions (Wadhwa 2001; Herd et al. 2002; McCanta et al. 2004; Karner et al. 2007b). The fO_2 of the cumulate Martian meteorites (Goodrich et al. 2003; Herd 2003) suggests they fall within a similar range as the basaltic shergottites. The range in fO_2 exhibited by the Martian meteorites suggests they are unique among the currently available suite of extra-terrestrial planetary materials.

Determining fO_2 in the Martian meteorites is a complicated process due to the geologic conditions the rocks experienced both during crystallization and subsequent ejection from the planetary surface. Although the basaltic shergottites resemble terrestrial basalts, many other Martian samples are predominantly cumulate in nature, a condition inferred to have resulted from slow cooling (e.g., Stolper and McSween 1979). Slow cooling may have compromised oxide oxybarometry as it has been demonstrated that Fe-Ti oxides can reequilibrate in the subsolidus (Lindsley et al. 1991; Treiman and Irving 2008), leading to non-magmatic fO_2 estimates (Ghosal et al. 1998). Reequilibration may also have affected other oxybarometers, such as olivine-pyroxene-spinel (Herd et al. 2001). Additionally, the lack of a remaining melt phase rules out melt-based fO_2 methods. Finally, the fact that many meteorites have experienced high shock pressures is an added complication (e.g., Stöffler et al. 1986; Langenhorst et al. 1991; Ikeda 1994).

Although some Martian meteorites do retain evidence of their high temperature crystallization conditions (e.g., Goodrich et al. 2003), a new oxybarometer was calibrated using the Eu content of Ca-pyroxenes and their coexisting melts (McKay et al. 1994; Wadhwa 2001; Musselwhite and Jones 2003; McCanta et al. 2004; Makishima et al. 2007) in order to study the fO_2 in all types of Martian meteorites. Europium is a multivalent element, existing as both Eu^{2+} and Eu^{3+}. As fO_2 increases, the amount of Eu^{3+} in the melt increases; as fO_2 decreases, Eu^{3+} in the melt decreases. Ca-pyroxene fractionates Eu^{2+} and Eu^{3+} as a function of composition, mainly Ca and Al content (e.g., Schosnig and Hoffer 1998; Shearer et al. 2006). The ratio of partition coefficients is less susceptible to variations in phase composition (e.g., Al content of pyroxene) than are individual partition coefficients (McKay et al. 1994), therefore the Eu-oxybarometer uses the relationship $D(Eu/Sm)_{pyroxene/melt} = (Eu/Sm)_{pyroxene}/(Eu/Sm)_{melt}$ as a measure of fO_2. Since Sm is monovalent and unaffected by changes in fO_2, changes in the Eu/Sm ratios with fO_2 reflect changes in the Eu^{2+}/Eu^{3+} ratio. As shown in previous studies (i.e., McKay et al. 1994; McCanta et al. 2004), $D(Eu/Sm)_{pyroxene/melt}$ increases as the system fO_2 increases and decreases as the system fO_2 decreases.

The pyroxene Eu-oxybarometer is a powerful tool for calculating fO_2 values in igneous rocks. For several reasons it is useful in situations where other oxybarometers (i.e., Fe-Ti oxides, glass Fe^{3+}/Fe^{2+}) are not available or reliable. First, the distribution of REE between pyroxene and melt is a function of fO_2 and this ratio is thought to be less susceptible to post-magmatic resetting than the iron redox ratio (Cherniak 2001; Van Orman et al. 2001). This is important for the Martian meteorites as many appear to have cooled slowly (e.g., McSween 1994). Second, the Eu-oxybarometer is well-calibrated for augite and pigeonite, two phases which arrive early on the liquidus in the Martian meteorites. This allows for investigation into the earliest history of the crystallizing melt. It should be noted that the pyroxene Eu-oxybarometer can only be used when plagioclase is not part of the crystallizing assemblage, as plagioclase has such a strong affinity for Eu^{2+}. Fortunately, Ca-pyroxene is on the liquidus of most Martian meteorite parental magmas significantly earlier than plagioclase (e.g., Stolper and McSween 1979; Longhi and Pan 1989; Minitti and Rutherford 2000).

Although the Eu-oxybarometer is extremely useful in calculating the fO_2 of many of the Martian meteorites as they crystallized, there is one major issue to be dealt with. Use of the Eu-oxybarometer relies on accurate knowledge of the REE content of both the pyroxene phenocrysts and the

equilibrium melt composition. Melt is rarely present in these meteorites, thus melt values for the trivalent REEs must often be retrieved from melt + crystal assemblages (which may have suffered chemical reequilibration) through calculations involving partition coefficients and inversion of phenocryst REE values. Since the basaltic shergottites appear to represent basaltic magmas that were crystallized at shallow depths or in lava flows (and therefore were only minimally affected by phenocryst accumulation and reequilibration (e.g., McCoy et al. 1992; McSween 1994)), this method is likely robust (Lundberg et al. 1988; Wadhwa et al. 1994, 2001; McSween et al. 1996). For other Martian meteorites, such as the slowly cooled intrusives, the lherzolitic shergottites, and the cumulate nakhlites, the assumption that early melt compositions can be accurately estimated using compositions of later crystallizing phases is less well demonstrated. These meteorites appear to have undergone significant crystal fractionation (e.g., McSween et al. 1979; Harvey et al. 1993) and their final bulk REE composition may no longer reflect the melts from which they crystallized. Although previous analytical studies have suggested that the bulk rock REE composition and the parent melt REE composition calculated by inverting the pyroxene core REE values are similar (Wadhwa et al. 2004), direct measurements of parent melt composition for the lherzolitic shergottites and nakhlites are not readily available. Because this melt data has been lacking, the Eu-oxybarometer has not been systematically applied to either the lherzolitic shergottites or nakhlites.

A potential way to directly access equilibrium melt compositions in the slowly cooled and cumulate Martian meteorites is provided by melt inclusions, which are melts trapped inside phenocrysts during crystallization. However, melt inclusions in these meteorites are sparse and in most cases have experienced significant post-entrapment crystallization and reequilibration (Johnson et al. 1991; Ikeda 1998; Varela et al. 2001; Goodrich and Harvey 2002; Stockstill et al. 2005). Therefore, to measure the REE composition of the melt, the inclusions must first be rehomogenized (e.g., Gaetani and Watson 2000; Varela et al. 2001; Danyushevsky et al. 2002; Stockstill et al. 2005). The research presented here focuses on nakhlite MIL 03346 and lherzolitic shergottite ALH 77005, both of which have had melt inclusions experimentally rehomogenized (Rutherford et al. 2005; Calvin and Rutherford 2008).

Two issues may affect the veracity of the melt inclusion compositions. First, during rehomogenization the daughter crystals and potentially some of the host phase are remelted to reproduce the original melt composition. The amount of host phase melt back is critical as it affects both the major and trace element concentrations. Eu^{3+}, Sm, and Gd are not substantially fractionated by the melt inclusion host phases studied, olivine or Ca-pyroxene (Colson et al. 1988; Wood and Blundy 1997; Borg and Draper 2003; Blinova and Herd 2008). While Eu^{2+} has the potential to be fractionated by pyroxene (e.g. Shearer et al. 2006), most Martian samples do not reach fO_2 values where Eu^{2+} is the dominant species. Experimental studies bear this out, with $DEu_{pyroxene}$ values (measured Eu is total Eu [$Eu^{2+} + Eu^{3+}$]) similar to $DSm_{pyroxene}$ and $DGd_{pyroxene}$ (Musselwhite et al. 2004; Blinova and Herd 2008). Therefore, too little or too much melt back of the host phases should not greatly change the REE concentration of the melts produced. Second, post-entrapment reequilibration can result in melt compositions that are not indicative of the original composition (e.g., Qin et al. 1992). The high cooling rates experienced by MIL 03346 indicate that reequilibration is likely not an issue. Fe-Mg reequilibration in ALH 77005 olivine would potentially result in all olivine phenocrysts throughout the sample sharing the same composition (similar to that seen in high metamorphic grade chondrites). Previous studies of ALH 77005 have observed grain to grain major element compositional variations in olivine (Ikeda 1994; Calvin and Rutherford 2008) implying that major element diffusive reequilibration was not complete. As Fe-Mg diffusion is faster than REE diffusion in olivine, these results suggest that post-entrapment reequilibration of the studied melt inclusions is not significant for the REEs. Additionally, ALH 77005 still retains sharp igneous oscillatory phosphorus zoning suggesting that phosphorus has not been diffusively reequilibrated (Milman-Barris et al. 2008; Beckett et al. 2008). Therefore, some incompatible elements are retained within the olivine despite the cooling history. Although $DP_{olivine}$ is not well constrained for comparison with $DREE_{olivine}$, the retention of sharp igneous P zonation suggests that the REEs in the melt inclusions have likely not been modified.

The objective of this study is to expand the application of the Eu-oxybarometer to the lherzolitic shergottites and nakhlites through analysis of the REE content of rehomogenized melt inclusions and to evaluate the relationship between bulk rock and parent melt REE compositions. The melt REE concentrations serve as input into the Eu-oxybarometer, providing new estimates of the crystallization fO_2 of these two meteorites. The method is also applied to other cumulate Martian meteorites thus expanding the range of fO_2 estimates for Mars magmas. In addition, the origin of the measured fO_2 values is investigated to determine which geologic processes may create the range of fO_2 values. The data generated provides new constraints on the heterogeneous geochemistry of the Martian interior and the origin of the fO_2 range present in the Martian meteorites.

METHODS

Experimental Methods

All experiments in this study were performed in the experimental petrology laboratory at Brown University. Experiments were run on approximately 1 mm^3 chips of

Table 1. Experimental conditions.

	T (°C)	P (MPa)	Time (hours)	fO_2 (ΔIW)
CC1-05-6	1165	80	23	0.5
CC1-05-7	1160	80	24	0.5
CC1-05-11	1150	80	48	0.5
Na-2	1115	160	48	1.5
Na-5	1135	160	24	1.5
Na-6	1110	70	72	1.0
Na-7	1110	70	72	3.5

each meteorite which were rehomogenized in TZM (titanium-zirconium-molybdenum) pressure vessels in sealed Pt-tubes (Rutherford et al. 2005; Calvin and Rutherford 2008). Samples were enclosed in graphite powder that generates a G-CO mixture through C reaction with the oxidized sample, thereby fixing the fO_2 at low values between iron wustite (IW) and quartz-fayalite-magnetite (QFM) depending on the pressure of the experiment. Additionally, the presence of graphite minimizes Fe loss to the Pt capsule. Rehomogenizations were run at pressures of 10s of MPa to 160 MPa and temperatures ranging from 1110° to 1165 °C (Table 1). Experiments were run for 24 to 72 hours to maximize reequilibration time. Olivine and pyroxene REE diffusion coefficients representative of the rehomogenization times in these experiments indicate that the melt inclusion REEs, unlike some of the major elements, would not have had time to reequilibrate with the surrounding mineral phase (van Orman et al. 2001; Cottrell et al. 2002). All samples were rapidly quenched, thin sectioned, and polished for analysis.

Analytical Methods

Experimentally rehomogenized glasses were analyzed for their major element compositions on the Johnson Space Center and Brown University Cameca SX-100 electron microprobes. Glass analyses were obtained using a 15 kV acceleration voltage, 20 nA beam current, and a partially defocused beam (diameter = 2–5 μm). Natural mineral and glass standards were used for calibration.

Measurements of pyroxene and glass REE compositions were obtained using the Arizona State University Cameca 6F ion microprobe (SIMS). Glass run products were analyzed using a 60–100 V offset, a beam current of 2 nA, and a beam size of ~10–15 μm. Pyroxenes were analyzed using a 60–100 V offset, a beam current of 5 nA, and a beam size of 50 μm. Natural volcanic glass standards were used for the glass calibration and natural mineral standards were used for the pyroxene calibration. Distribution coefficients were calculated from REE/^{30}Si intensity ratios. A minimum of six spots per glass phase were analyzed for each experiment. REE values in the MIL 03346 pyroxenes are composed of the average of two spots.

PETROGRAPHY OF MIL 03346 AND ALH 77005

The two meteorites studied were MIL 03346 and ALH 77005. MIL 03346 is a nakhlite consisting of abundant Ca-rich pyroxene (cores: $En_{38}Fs_{21}Wo_{41}$; rims: $En_{9}Fs_{44}Wo_{47}$) and sparse olivine phenocrysts (cores: $Fo_{43.5}$; normally zoned rims) in a dark fine-grained groundmass of fayalitic olivine, Fe-rich Ca-pyroxene, Ti-magnetite, cristobalite, and apatite in order of decreasing abundance (e.g., Day et al. 2006; Imae and Ikeda 2007) (Fig. 1A). The pyroxene and olivine phenocrysts have large homogeneous cores surrounded by normally zoned rims (Day et al. 2006). The disequilibrium crystal textures in the holocrystalline groundmass indicate it experienced high cooling rates (Hammer and Rutherford 2005), while the fayalite, magnetite, and cristobalite phase assemblage suggests that the groundmass crystallized in an oxidizing environment compared to other nakhlites (e.g., Treiman 2005). MIL 03346 was chosen for study due to the presence of significant amounts of groundmass, potentially indicative of a late melt phase, and the observed presence of melt inclusions within the clinopyroxene grains.

ALH 77005 is a lherzolitic shergottite with poikilitic and non-poikilitic areas. Poikilitic areas consist of cumulus olivine ($Fo_{73.7}$) and chromite poikilitically enclosed by large low-Ca pyroxenes (cores: $En_{77}Fs_{19}Wo_{4}$; rims: $En_{65}Fs_{20}Wo_{15}$) with minor high-Ca pyroxene (cores: $En_{55}Fs_{15}Wo_{30}$; rims: $En_{48}Fs_{12}Wo_{40}$) (e.g., McSween et al. 1979; Wänke et al. 1986; Mikouchi and Miyamoto 2000) (Fig. 1B). The olivines are euhedral to subhedral with relatively homogeneous cores surrounded by thin rims of higher Fe olivine. Other portions of ALH 77005 are non-poikilitic and contain subhedral olivine ($Fo_{73.2}$) with interstitial regions composed of low-Ca (range: $En_{66}Fs_{27}Wo_{7}$ to $En_{61}Fs_{23}Wo_{16}$) and high-Ca (range: $En_{53}Fs_{15}Wo_{32}$ to $En_{48}Fs_{14}Wo_{38}$) pyroxene, maskelynite (range: $An_{58}Ab_{41}Or_{1}$ to $An_{48}Ab_{49}Or_{3}$), and other trace phases (McSween et al. 1979; Mikouchi and Miyamoto 2000). The documentation of melt inclusions in ALH 77005 in previous studies (e.g., Zipfel and Goodrich 2001; Goodrich and Harvey 2002) suggested that rehomogenization experiments on this sample would be fruitful.

RESULTS

Melt REE Concentrations

MIL 03346

Experiments conducted for this study resulted in rehomogenization of both melt inclusions in pyroxene phenocrysts (Fig. 1C) and groundmass melts. As MIL 03346 contains significant amounts of groundmass that may represent a melt composition in equilibrium with the relatively unzoned Ca-pyroxene phenocrysts (Rutherford et al. 2005; Day et al. 2006), REEs in both rehomogenized groundmass and melt inclusions (diameter >50 μm) were

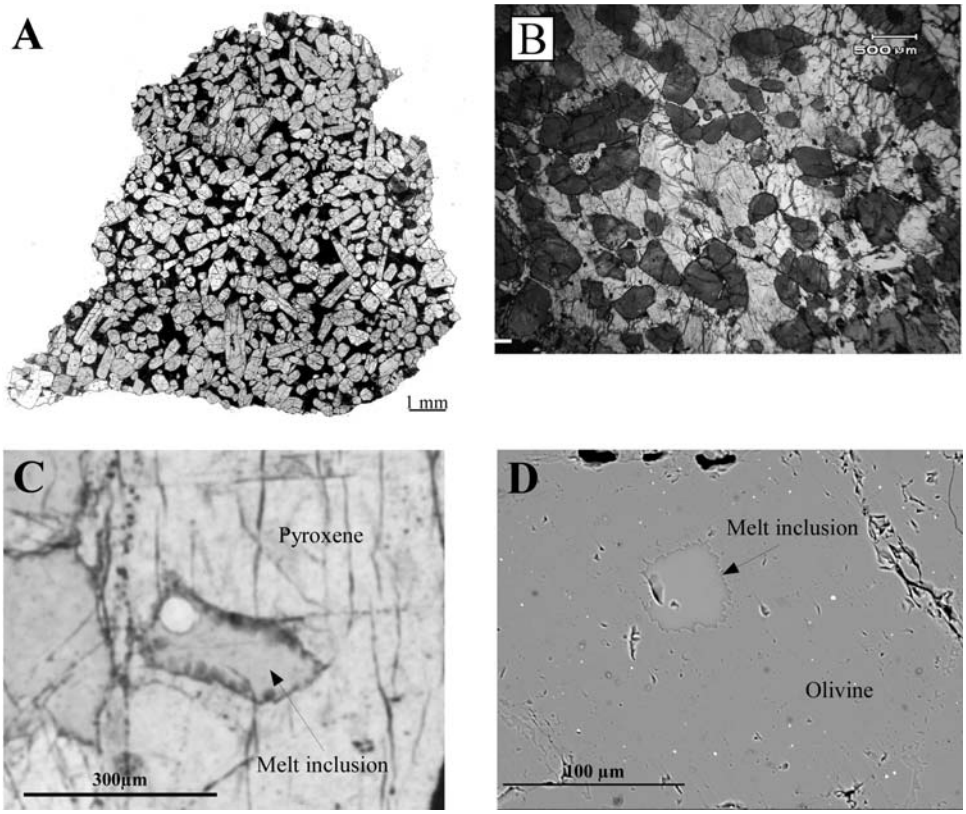

Fig. 1. Photomicrographs of MIL 03346 and ALH 77005 meteorites. Scale bars are shown on images. A) Photomicrograph mosaic of MIL 03346. The majority of the phenocrystic material is pyroxene. Only one olivine was found in this sample. The dark fine-grained groundmass consists of fayalitic olivine, Fe-rich Ca-pyroxene, Ti-magnetite, cristobalite, and apatite. B) Photomicrograph of ALH 77005. Darker crystals are olivine grains. Lighter interstitial material is pyroxene interspersed with opaque grains. C) Rehomogenized melt inclusion in pyroxene and groundmass in MIL 03346 at 20× magnification. D) Backscatter electron image of an experimentally rehomogenized olivine melt inclusion in ALH 77005.

measured. However, because of the potential of the groundmass to be affected by later changes in the magmatic regime, only melt inclusion REE compositions were used as representative early Martian melts in fO_2 calculations. To determine if rehomogenization was complete, the remelted composition was compared to the natural sample through analysis of the compositions of coexisting clinopyroxene and olivine (Rutherford and Hammer 2008). Major and rare earth element analyses of the MIL 03346 rehomogenized melt inclusions and groundmass are presented in Table 2. The two melt inclusions analyzed have similar major and trace element compositions. The close correspondence between the melt inclusion and groundmass compositions at 1125 °C suggests that there was little exchange between the melts trapped in the inclusions and the remaining melt subsequent to inclusion trapping (Rutherford and Hammer 2008).

Both the rehomogenized groundmass and the rehomogenized melt inclusions in MIL 03346 are enriched in REE relative to chondrites, although the inclusions are slightly more enriched (Fig. 2A). Both melt types are strongly LREE enriched (Ce/Yb ~4) (Fig. 2A). The REE abundances are comparable to whole rock data determined for MIL 03346 (Day et al. 2006), Nakhla (Lodders 1998), Lafayette (Dreibus et al. 2003), NWA 817 (Sautter et al. 2002), and Y 593/749 (Wadhwa et al. 2004), but the rehomogenized melts are enriched by a factor of 3–6 over the whole rock data (Fig. 2B). MIL 03346 melt REE concentrations are also similar in pattern and magnitude to the Nakhla parent melt calculated using REE pyroxene/melt partition coefficients (Wadhwa and Crozaz 1995) (Fig. 2C).

ALH 77005

Olivine-hosted melt inclusions in ALH 77005 generally contained high-Ca pyroxene and plagioclase crystals and SiO_2-rich regions prior to rehomogenization. Experiments produced both partially and totally rehomogenized melt inclusions in ALH 77005 olivine phenocrysts (Fig. 1D; Table 3), as well as some melting of the matrix between grains. Criteria including experimental length (run time between 48 and 72 hours) and melt-olivine K_D (experimental average = 0.27; K_D for melts in equilibrium with olivine ~0.30 [Roeder 1974]) were used to determine if the experiment approached equilibrium (Calvin and Rutherford 2008). REE measurements were made on totally

Table 2. Representative analyses of MIL 03346 pyroxenes and experimentally rehomogenized melts.

	Avg. melt inclusion	Na-2 matrix melt	Na-5 matrix melt	Na-6 matrix melt	Na-7 matrix melt	Pyroxene
SiO_2	49.91 (0.53)	49.20 (0.30)	49.34 (0.26)	50.80 (0.20)	51.70 (0.22)	51.02 (0.35)
TiO_2	1.55 (0.12)	1.64 (0.08)	1.35 (0.03)	1.60 (0.10)	1.12 (0.03)	0.26 (0.05)
Al_2O_3	9.78 (0.69)	9.02 (0.20)	9.20 (0.15)	9.80 (0.15)	9.35 (0.15)	0.91 (0.05)
FeO	24.82 (0.81)	23.13 (0.35)	22.89 (0.25)	21.36 (0.20)	22.30 (0.17)	13.17 (0.14)
MgO	1.74 (0.74)	3.19 (0.17)	3.51 (0.13)	2.90 (0.10	2.50 (0.03)	12.70 (0.20)
CaO	8.09 (0.53)	9.20 (0.18)	9.35 (0.12)	9.14 (0.13)	8.10 (0.11)	19.21 (0.20)
Na_2O	2.27 (0.62)	2.60 (0.25)	2.58 (0.02)	2.90 (0.12)	2.74 (0.05)	0.27 (0.05)
K_2O	0.81 (0.11)	0.76 (0.06)	0.73 (0.03)	0.87 (0.06)	0.75 (0.06)	ND
MnO	0.45 (0.06)	0.49 (0.09)	0.44 (0.05)	0.55 (0.05)	0.55 (0.05)	0.44 (0.03)
P_2O_5	0.64 (0.07)	0.78 (0.12)	0.63 (0.03)	0.63 (0.10)	0.67 (0.03)	ND
Cr_2O_3	ND	0.02 (0.02)	0.03 (0.02)	0.02 (0.02)	0.02 (0.01)	0.31 (0.05)
	100.06	100.03	100.05	100.57	99.80	98.29
La	10.32 (0.14)	8.73 (0.60)	8.23 (0.37)	12.45 (0.36)	13.75 (0.63)	0.35 (0.04)
Ce	26.97 (0.25)	23.03 (1.50)	21.63 (0.60)	32.98 (5.28)	34.47 (1.66)	1.73 (0.20)
Pr	4.16 (0.09)	3.49 (0.25)	3.32 (0.14)	3.77 (0.06)	5.48 (0.29)	0.32 (0.03)
Nd	19.01 (0.20)	15.15 (2.56)	15.21 (0.29)	15.99 (0.02)	23.11 (0.30)	1.85 (0.15)
Sm	4.05 (0.14)	3.41 (0.36)	3.27 (0.29)	3.41 (0.01)	5.05 (0.16)	0.61 (0.01)
Eu	1.20 (0.07)	1.13 (0.05)	1.07 (0.06)	1.13 (0.02)	1.40 (0.08)	0.19 (0.01)
Gd	3.68 (0.22)	3.26 (0.42)	3.01 (0.16)	3.41 (0.27)	4.43 (0.08)	0.68 (0.03)
Tb	0.55 (0.04)	0.48 (0.03)	0.46 (0.01)	0.50 (0.03)	0.75 (0.07)	0.11 (0.01)
Dy	3.60 (0.10)	3.14 (0.40)	2.93 (0.09)	3.15 (0.14)	4.34 (0.06)	0.72 (0.04)
Ho	0.74 (0.04)	0.64 (0.06)	0.61 (0.01)	0.63 (0.03)	0.92 (0.02)	0.14 (0.01)
Er	2.10 (0.08)	1.82 (0.26)	1.67 (0.01)	1.82 (0.07)	2.53 (0.01)	0.37 (0.01)
Tm	0.26 (0.03)	0.25 (0.03)	0.25 (0.01)	0.27 (0.01)	0.40 (0.02)	0.05 (0.01)
Yb	1.97 (0.08)	1.65 (0.25)	1.60 (0.04)	1.72 (0.04)	2.30 (0.11)	0.39 (0.03)
Lu	0.31 (0.04)	0.25 (0.02)	0.25 (0.01)	0.26 (0.02)	0.33 (0.02)	0.06 (0.01)

All Fe as FeO. Major elements are reported as weight percents. REEs are reported as ppm. Numbers in parentheses represent one standard deviation from the mean.
ND = Not detected.

rehomogenized olivine-hosted melt inclusions (diameter >50 μm) and groundmass melts (Calvin and Rutherford 2008). Although the melt contained in olivine-hosted inclusions does not represent the most primitive melts measured in ALH 77005 (Goodrich and Harvey 2002), they do represent magmas that were trapped during olivine crystallization early in the crystallization sequence and therefore can be studied to understand the REE concentrations in ALH 77005 melts. Additionally, several olivine-hosted melt inclusions with anomalous high phosphorus values (and correlated high Ca) were measured by Calvin and Rutherford (2008). Melt inclusions with high P_2O_5 may represent either slow growth of olivine along the inclusions wall allowing phosphorus to diffuse away from the growth zone into the melt and/or selective dissolution of high phosphorus olivine and reprecipitation of low phosphorus olivine, with the excess phosphorus partitioned into the melt (Milman-Barris et al. 2008). This may lead to phosphate crystallization within the melt inclusion. As phosphates are the container for significant REEs in these samples, care was taken to avoid these high P_2O_5 inclusions when analyzing for REE content.

As the ALH 77005 meteorite is predominantly holocrystalline with little groundmass, the interstitial melt REEs were found to have a wide-range in composition (Edmunson et al. 2005) and are believed to have questionable relevance to the early crystallizing magma. Although REE values in both regions were measured (Table 3), only REE measured in melt inclusions were used as representative Martian melt compositions in later calculations.

Major and rare earth element analyses of the ALH 77005 rehomogenized melt inclusions and groundmass melts are presented in Table 3. The two types of melts show similar REE enrichments and patterns (Fig. 3A), although the inclusion REE values are slightly higher than those measured in the groundmass. REEs in both melts are enriched relative to chondritic values (Anders and Grevasse 1989). The concentration pattern appears to be unfractionated from La to Pr, to increase from Pr to Gd (Gd/Pr ~2.6), to remain constant from Gd to Dy, and to decrease from Dy to Lu (Dy/Lu ~1.4). The shape of the REE plot is consistent with whole rock REE concentrations determined for ALH 77005 (Ma et al. 1981; Smith et al. 1984; Dreibus et al. 1992) and for other lherzolitic shergottites, such as LEW 88516 (Dreibus et al. 1992) and Y793605 (Warren and Kallemeyn 1997) (Fig. 3B). However, both the rehomogenized melt inclusion and groundmass melt concentrations are more enriched than the whole rock values (Fig. 3B).

Additionally, calculated lherzolitic shergottite parent melt compositions (Lundberg et al. 1990; Harvey et al. 1993) are also similar in REE pattern to the melts measured in this study (Fig. 3C). The parent melt compositions were calculated using both low and high-Ca pyroxene distribution coefficients (Lundberg et al. 1990; Harvey et al. 1993).

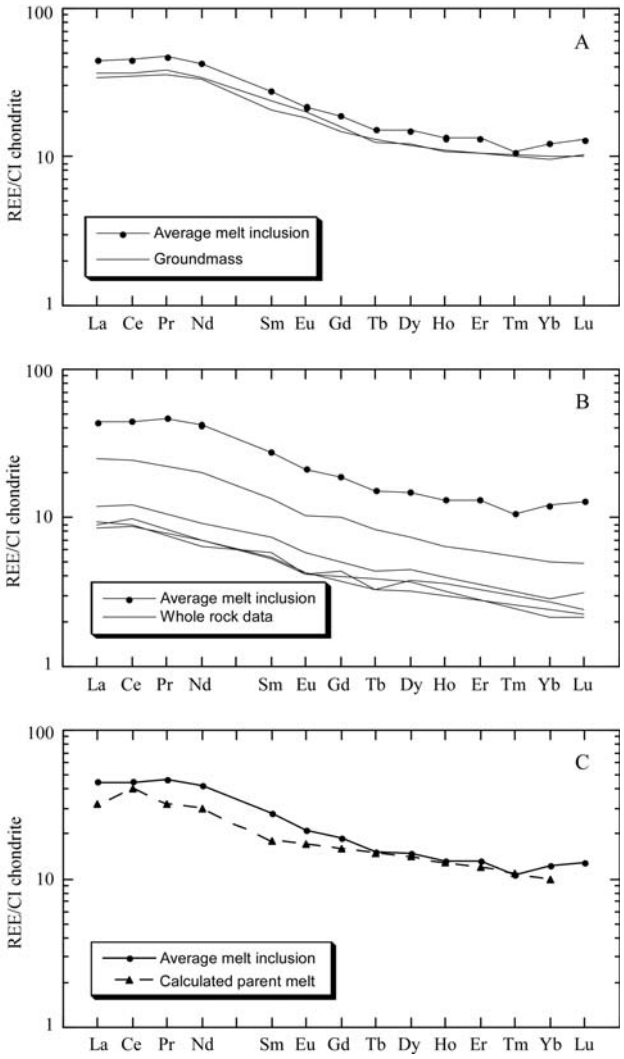

Fig. 2. MIL 03346 rehomogenized melt inclusion REE composition. A) Chondrite normalized plot of REE concentrations in rehomogenized melt inclusions and groundmass melts in MIL 03346. Both melts have similar patterns, although the melt inclusion REE content is measurably higher. This is likely due to due to each sampling the magma at a different stage of crystallization. B) Chondrite normalized plot of MIL 03346 REE concentrations in rehomogenized melt inclusions and whole rock REE contents for Nakhla (Lodders 1998), MIL 03346 (Day et al. 2006), Lafayette (Dreibus et al. 2003), NWA 817 (Sautter et al. 2002), and Y593/749 (Wadhwa et al. 2004). The REE composition of the melt inclusions has a similar REE pattern to that of the whole rocks, but shows significant enrichment. C) Chondrite normalized plot of average MIL 03346 REE concentrations in rehomogenized melt inclusions and groundmass melts and the calculated Nakhla parent melt of Wadhwa and Crozaz (1995). The REE patterns are parallel to sub-parallel. Normalization values from Anders and Grevasse (1989).

Calculation of parent melt composition from chemically equilibrated samples such as ALH 77005 can result in erroneous interpretations (Treiman 1996). However, although olivines in ALH 77005 are chemically equilibrated with respect to their major elements, recent studies have shown

Table 3. Representative analyses of ALH 77005 experimentally rehomogenized melts.

	CC1-05-6A MI[a]	CC1-05-7A MI	CC1-05-11A MI	CC1-05-6 GM	CC1-05-7 GM	CC1-05-11 GM
SiO_2	47.44 (0.37)	48.35 (0.22)	49.83 (0.45)	48.42 (0.57)	48.84 (0.32)	50.78 (0.41)
TiO_2	1.51 (0.08)	2.07 (0.12)	1.34 (0.07)	1.57 (0.07)	1.08 (0.08)	1.22 (0.15)
Al_2O_3	10.41 (0.64)	14.38 (0.38)	12.62 (0.54)	11.85 (0.91)	15.75 (0.31)	13.95 (0.19)
FeO*	15.55 (0.65)	15.28 (0.17)	13.46 (0.22)	13.30 (0.66)	11.92 (0.42)	9.81 (0.28)
MgO	6.83 (0.20)	5.37 (0.13)	5.31 (0.31)	7.26 (0.25)	6.50 (0.19)	5.98 (0.24)
CaO	11.60 (0.32)	11.07 (0.25)	10.11 (0.33)	10.26 (0.55)	8.71 (0.15)	9.84 (0.28)
Na_2O	1.94 (0.27)	2.08 (0.34)	2.67 (0.18)	2.23 (0.14)	2.88 (0.30)	2.87 (0.36)
K_2O	0.22 (0.08)	0.09 (0.02)	0.64 (0.05)	0.25 (0.11)	0.19 (0.06)	0.60 (0.05)
MnO	0.46 (0.06)	0.45 (0.05)	0.34 (0.06)	0.39 (0.05)	0.38 (0.08)	0.33 (0.09)
	95.96	99.14	96.32	95.53	96.25	95.38
La	1.90 (0.06)	1.44 (0.05)	1.32 (0.07)	1.50 (0.01)	0.89 (0.03)	1.61 (0.04)
Ce	4.25 (0.11)	3.47 (0.08)	3.78 (0.12)	3.45 (0.18)	2.14 (0.05)	3.74 (0.06)
Pr	0.68 (0.04)	0.61 (0.03)	0.48 (0.04)	0.54 (0.03)	0.36 (0.02)	0.59 (0.02)
Nd	3.93 (0.10)	3.56 (0.08)	2.70 (0.10)	3.10 (0.21)	1.92 (0.05)	3.15 (0.06)
Sm	2.12 (0.10)	1.86 (0.08)	1.58 (0.10)	1.77 (0.14)	1.14 (0.05)	1.78 (0.06)
Eu	1.03 (0.05)	1.17 (0.04)	0.89 (0.05)	0.92 (0.04)	0.84 (0.03)	0.90 (0.03)
Gd	4.08 (0.18)	3.52 (0.14)	3.12 (0.17)	3.15 (0.27)	1.99 (0.08)	3.29 (0.10)
Tb	0.72 (0.04)	0.60 (0.03)	0.61 (0.05)	0.59 (0.07)	0.37 (0.02)	0.65 (0.03)
Dy	5.49 (0.12)	4.36 (0.09)	4.52 (0.13)	4.45 (0.44)	2.44 (0.05)	4.40 (0.07)
Ho	1.07 (0.05)	0.93 (0.04)	0.96 (0.06)	0.96 (0.09)	0.53 (0.02)	0.86 (0.03)
Er	3.35 (0.10)	2.46 (0.08)	2.81 (0.11)	2.57 (0.27)	1.31 (0.04)	2.52 (0.06)
Tm	0.43 (0.04)	0.36 (0.03)	0.46 (0.04)	0.37 (0.03)	0.17 (0.02)	0.32 (0.02)
Yb	3.11 (0.10)	2.26 (0.07)	2.54 (0.11)	2.33 (0.22)	1.30 (0.04)	2.30 (0.06)
Lu	0.39 (0.04)	0.36 (0.03)	0.35 (0.05)	0.36 (0.03)	0.15 (0.02)	0.32 (0.02)

All Fe as FeO. Major elements are reported as weight percents. REEs are reported as ppm. Numbers in parentheses represent one standard deviation from the mean.

[a]MI indicates the composition was measured in a melt inclusion. All other data comes from rehomogenized groundmass measurements.

they retain primary igneous oscillatory zoning of several trace elements, specifically P and Cr (Beckett et al. 2008; Milman-Barris et al. 2008). The presence of primary oscillatory zoning in trace elements indicates that trace elements have not been reequilibrated and therefore, that parent melt calculations may be valid. The higher parent melt REE composition for the high-Ca pyroxene, as well as petrographic relations, suggests that it began crystallizing later in the magmatic history (Lundberg et al. 1990). The high-Ca pyroxene parent melts provide a consistent match in both REE pattern and abundance to the inclusion melts analyzed, although the low-Ca pyroxene melts are less enriched.

DISCUSSION

Measured Rehomogenized Inclusion Melts versus Whole Rock REE Abundances

If a system evolves through closed-system processes (i.e., no mixing with new melts of different compositions, no assimilation of wallrock), the REE pattern of the parent melt and that of the whole rock should be parallel. In the basaltic shergottites, which appear as a group to have experienced less crystal accumulation than the lherzolitic shergottites or nakhlites, studies have found that the REE pattern of the proposed parent melt parallels that of the bulk rock, which implies closed-system evolution (Wadhwa et al. 1994). The inferred slow cooling and cumulate nature of the lherzolitic shergottites and the nakhlites suggests that, unlike the basaltic shergottites, their whole rock REE values may not be parallel to those of the melts from which they crystallized. To investigate this possibility, the REE compositions measured in the rehomogenized melt inclusions were compared to whole rock measurements from previous works (Figs. 2B, 3B). It is clear from these figures that the rehomogenized melt inclusion REE patterns trend parallel to the whole rock patterns (e.g., average La/Sm for MIL 03346 rehomogenized melt inclusions is 2.55; average bulk rock La/Sm is 2.70). The cumulate nature of these meteorites does not affect the parallelism of their rehomogenized melt and whole rock REE patterns as the minerals settling in the cumulus pile (pyroxene or pyroxene + olivine) would lower the total REE content of the whole rock, but would not significantly change the shape of the REE pattern of the parent melt. The correlation shown above suggests that the whole rock REE compositions of other cumulate Martian meteorites may also parallel that of their parent melt and that the whole rock REE pattern can be used as a proxy for the parent melt REE pattern. For the Eu-oxybarometer fO_2 estimates presented in the next section, the assumption of the parallel nature of whole rock and parent melt REE patterns is applied to other lherzolitic shergottites and nakhlites in order to determine their melt (Eu/Sm) ratios.

Previous studies have calculated Martian meteorite parent melt REE concentrations in meteorites that no longer

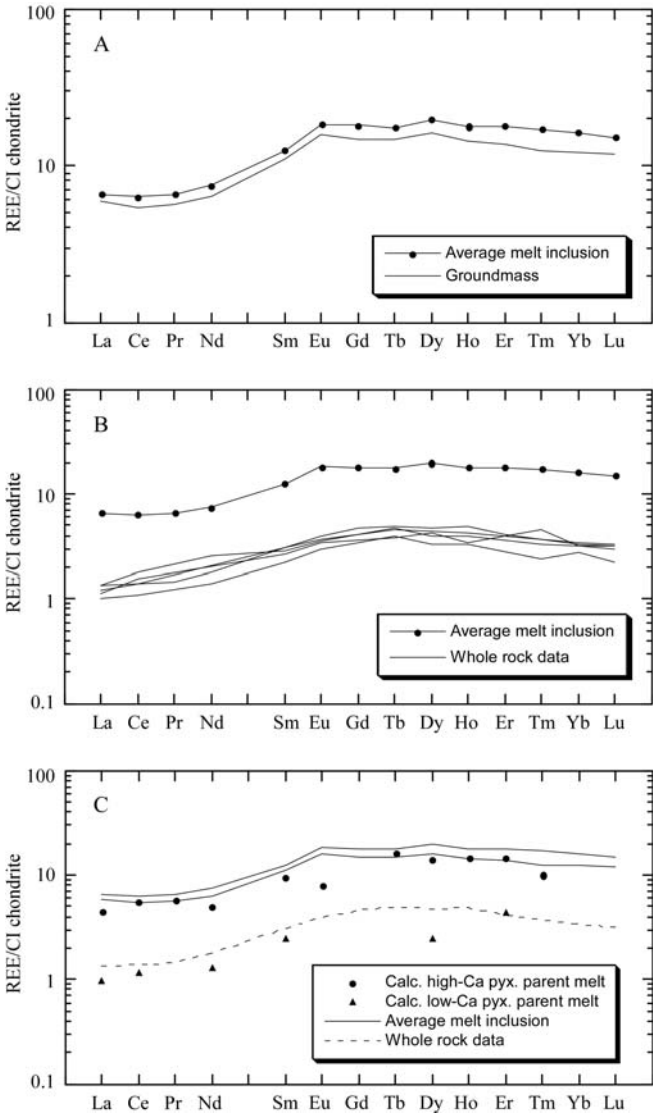

Fig. 3. ALH 77005 rehomogenized melt inclusion REE composition. (A) Chondrite normalized plot of REE concentrations in rehomogenized melt inclusions and groundmass melts in ALH 77005. Both melts have similar patterns, although the melt inclusion REE content is measurably higher. As with the MIL 03346 data, this is likely due to each sampling the magma at a different stage of crystallization. (B) Chondrite normalized plot of REE concentrations in rehomogenized melt inclusions and whole rock REE contents for ALH 77005 (Ma et al. 1981; Smith et al. 1984; Dreibus et al. 1992) and other lherzolitic shergottites (LEW 88516: Dreibus et al. 1992; Y793605: Warren and Kallemeyn 1997). The REE composition of the melt inclusions has a similar REE pattern to that of the whole rocks, but shows significant enrichment. (C) Chondrite normalized plot of REE concentrations in rehomogenized melt inclusions and groundmass, the calculated ALH 77005 parent melt compositions from both high and low-Ca pyroxene distribution coefficients (Lundberg et al. 1990), and the ALH 77005 whole rock composition (Smith et al. 1984). The rehomogenized melts have a similar REE pattern to the low-Ca pyroxene calculated parent melt, but are more enriched. However, the high-Ca pyroxene parent melt is consistent in both REE pattern and magnitude to the melts in this study. Normalization values from Anders and Grevasse (1989).

have melt (i.e., glass) present (Lundberg et al. 1990; Wadhwa et al. 1994; Beck et al. 2006). This is commonly done in pyroxene-bearing samples that appear to have retained their original magmatic REE zonation. Melt REE concentration calculations are made using pyroxene core compositions and appropriate pyroxene mineral/melt partition coefficients and inverting for equilibrium melt composition (i.e., Wadhwa et al. 1994). With the new data presented above, an evaluation of the partition coefficient method for determining parent REE concentration can be made. For both ALH 77005 and MIL 03346, the calculated parent melt REE composition is similar in shape and magnitude to the melt compositions measured in the rehomogenized melt inclusions (Figs. 2C, 3C). This suggests that the high-Ca pyroxenes in these meteorites have retained their primary igneous REE zonation and have not been affected by secondary processes. Therefore for these cumulate meteorites, the equilibrium melt REE composition calculations made relying on the high-Ca pyroxene partition coefficients yield values that are near those actually measured in the rehomogenized melt inclusions.

Use of the Eu-Oxybarometer

In order to apply the Eu-oxybarometer to a sample, the REE composition of both the crystallizing pyroxene and the coexisting melt must be well constrained. With the new melt REE data presented above and the recognition of the similarity between REE values calculated using distribution coefficients and trapped melt inclusions, this oxybarometer can now be used to investigate a larger group of Martian meteorites. However, the chemical composition of the pyroxenes must be detailed to constrain potential errors. As mentioned above, only pyroxene REE values measured prior to the onset of plagioclase crystallization can be used, therefore only core compositions are utilized below. Additionally, several other issues must be addressed. First, substitution of minor elements in addition to the REEs, most notably Al and potentially Fe^{3+}, has been demonstrated to have an effect on pyroxene REE partitioning (Lundstrom et al. 1998; Schwandt and McKay 1998; Shearer et al. 2006). To minimize the effect of these substitutions, the concentration of multivalent Eu is ratioed to the trivalent cation Sm in all oxybarometer calculations (i.e., McKay et al. 1994). Moreover, the measured Fe^{3+} content of the MIL 03346 pyroxenes appears uniformly low when measured by single crystal Mössbauer spectroscopy (Domeneghetti et al. 2006). Second, although the Eu-oxybarometer has been calibrated for both $D(Eu/Sm)_{pyx/melt}$ and $D(Eu/Gd)_{pyx/melt}$ (Musselwhite and Jones 2003; McCanta et al. 2004; Makishima et al. 2006), SIMS measurements of Gd in the natural samples are hampered by the low abundance of Gd in the pyroxenes (parts per billion: i.e., Wadhwa et al. 1994; Wadhwa and Crozaz 1995) and ion interferences with other elements (e.g., Zinner and Crozaz 1986). Therefore, Gd cannot be directly measured by SIMS in the natural pyroxenes and its abundance must be calculated by interpolation (Zinner and Crozaz 1986). As the calibrations were generally run on REE-doped samples, these issues were not encountered. However, natural sample compositions are necessary as input into the Eu-oxybarometer and the errors encountered when using reported natural Gd concentrations can be large (e.g., McCanta et al. 2004). To avoid these analytical issues, only the $D(Eu/Sm)_{pyx/melt}$ oxybarometer is used in this study to take advantage of the fact that both elements were directly measured. Finally, the accuracy of the Eu-oxybarometer decreases markedly around an fO_2 of QFM. This results from the essentially total oxidation of Eu^{2+} to Eu^{3+} under these fO_2 conditions (e.g., McKay et al. 1994; McCanta et al. 2004). The slope of the oxybarometer calibration curve begins to flatten at this juncture preventing extrapolations to higher fO_2's. As a result of this flattening, the errors on the fO_2 estimated increase near QFM. Whereas errors of ±0.3 log units fO_2 are calculated for fO_2 values between IW−1 and IW+3, errors of ±0.6 log units fO_2 are calculated for fO_2 values greater than IW+3 (for reference, QFM = IW+3.5).

Crystallization fO_2 Calculations

To determine the fO_2 conditions experienced in the earliest crystallizing melt, melt inclusion REE abundances in ALH 77005 were combined with previously determined REE concentrations for ALH 77005 poikilitic low-Ca pyroxene cores (Wadhwa et al. 1994). Low-Ca pyroxene was used as it is one of the earliest phases crystallizing on the shergottite liquidus (e.g., Stolper and McSween 1979; McSween et al. 1996; Minitti and Rutherford 2000; Dann et al. 2001) and so should preserve the early history of the magma. Core values were used to insure that the pyroxene REE values were measured in material that had not crystallized in the presence of plagioclase, a later liquidus phase (Minitti and Rutherford 2000). The low-Ca pyroxene calibration of the Eu-oxybarometer of McCanta et al. (2004) was employed for these calculations. These calculations indicate a crystallization fO_2 for this magma of IW+1.1 (±0.3). As given in Fig. 4, this fO_2 lies within the range of values measured in the basaltic shergottites (IW−0.6 to IW+1.9; McCanta et al. 2004).

The Eu-oxybarometer was also applied to MIL 03346 using melt and pyroxene REE concentrations determined in this study. The nakhlites are dominated by high-Ca pyroxene, rather than low, therefore high-Ca pyroxene REE compositions and the Eu-oxybarometer calibrations for high-Ca pyroxene (Musselwhite and Jones 2003; Makishima et al. 2006, 2007) were used. The Musselwhite and Jones (2003) calibration for a basaltic shergottite composition was used in

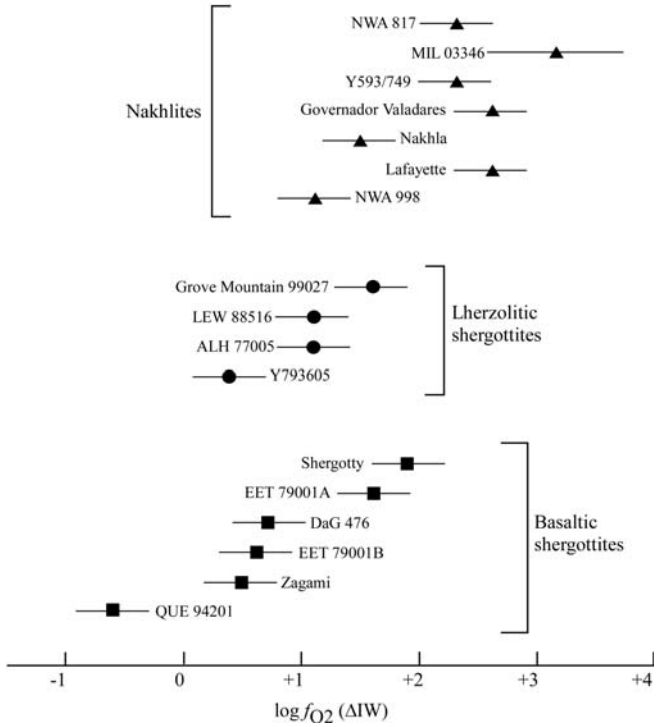

Fig. 4. Range of fO_2 values present in the SNC meteorites determined using the Eu-oxybarometer on both low and high-Ca pyroxene. Basaltic shergottite data are from McCanta et al. (2004) and Musselwhite and Jones (2003). Data for the lherzolitic shergottites and nakhlites are from this study. Nakhlites are plotted in relative depth order (NWA 998 = deepest) using the single flow model of Mikouchi et al. (2003).

all augite fO_2 calculations in this study as it was calibrated for $D(Eu/Sm)_{pyx/melt}$. Although this calibration is based on a starting composition different than that of the nakhlites, comparison to the original angrite calibration (McKay et al. 1994) suggests that application to the nakhlites is reasonable (Musselwhite and Jones 2003). The Makishima et al. (2006; 2007) oxybarometer is not utilized as it was only well-calibrated for $D(Eu/Gd)_{pyx/melt}$. In addition to the problems with Gd measurements mentioned above, many bulk rock measurements in the literature do not include Gd concentrations, making it difficult to use the Makishima et al. (2007) barometer for such samples. As in the ALH 77005 calculations, only pyroxene core REE values were used to satisfy the condition necessary for use of the Eu-oxybarometer that plagioclase not be a co-crystallizing phase. MIL 03346 records a crystallization fO_2 of IW+3.2 (±0.6). This is the highest fO_2 value estimated for any pyroxene core in the Martian meteorites and indicates that relatively oxidizing conditions are present in the Martian interior, or at least at the depth where phenocrysts grew in this nakhlite.

With the recognition that the whole rock REE patterns are similar to the early melt compositions measured in rehomogenized melt inclusions, the whole rock values, as well as pyroxene values from earlier studies, can be used as

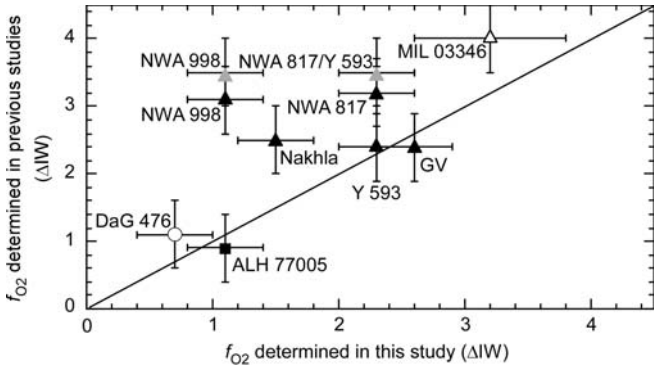

Fig. 5. Comparison of fO_2 values in the nakhlites and lherzolitic shergottites determined in this study using the Eu-oxybarometer and those from previous studies using a variety of methods (filled square: Goodrich et al. 2003 (olivine-pyroxene-spinel oxybarometry); open circle: Herd 2003 (olivine-pyroxene-spinel oxybarometry); grey triangles: Wadhwa et al. 2004 (qualitative assessment of Eu/Gd distribution); filled triangle: Makishima et al. 2007 (FeTi-oxide thermobarometry); open triangle: Herd and Walton 2008 (crystallization experiments). GV = Governador Valadares, Y 593 = Y000593.

approximations in Eu-oxybarometer input for other cumulate Martian meteorites. In doing this, care was taken to select REE values for pyroxenes which had not been crystallizing in the presence of plagioclase. The crystallization fO_2 values calculated for the lherzolitic shergottites LEW 88516, Y793605, and Grove Mountain 99027 are IW+1.1, 0.4, and 1.6, respectively. These values are close to that of ALH 77005 and lie within the fO_2 region defined by the basaltic shergottites (Wadhwa 2001; Herd et al. 2002; McCanta et al. 2004) (Fig. 4). Many of the newly measured nakhlite fO_2 values are nearly as oxidizing as MIL 03346 (Governador Valadares [IW+2.6]; Lafayette [IW+2.6]; Y 593/749 [IW+2.3]; NWA 817 [IW+2.3]), although more reduced meteorites are also present (Nakhla [IW+1.5]; NWA 998 [IW+1.1]) (Fig. 4). The fO_2 range observed is a measure of the Eu/Sm ratios of the pyroxene cores. The ratios in Nakhla and NWA 998 are measurably lower than those in the other studied nakhlites and are well outside error estimations suggesting the fO_2 differences they record are real as well. A range of ~2.5 orders of magnitude in fO_2 are present in the nakhlites, similar to that seen in the basaltic shergottites. This new data extends the known total range of Martian meteorite magma crystallization conditions to four orders of magnitude.

Comparison with Previous fO_2 Estimates

A comparison of the fO_2 values of the nakhlites and cumulate shergottites from this study and previous studies (Goodrich et al. 2003; Herd 2003; Wadhwa et al. 2004; Makishima et al. 2007) is presented in Fig. 5. There appear to be good matches between the results from the Eu-oxybarometer for the shergottites (DaG 476, ALH 77005) and the shergottite data from other studies (specifically, the

olivine-pyroxene-spinel oxybarometer [filled square: Goodrich et al. 2003; open circle: Herd 2003]). This is not unexpected as both oxybarometers rely on early crystallizing phases and are therefore recording the fO_2 conditions in the early melts. Data for the nakhlites is more scattered when compared with FeTi oxide barometry (filled triangles: Makishima et al. 2007), a qualitative assessment of the pyroxene Eu/Gd distribution (grey triangles: Wadhwa et al. 2004), or the results of crystallization experiments (open triangle: Herd and Walton 2008). The oxide data for meteorites Y593 and Governador Valadares shows a relatively good correlation with data from this study. Nakhla, NWA 817, and MIL 03346 are offset from the 1:1 line, but define a similar slope. The major discrepancy lies with NWA 998; FeTi oxide barometry records this sample as significantly more oxidizing. As mentioned earlier, FeTi-oxides can undergo significant subsolidus reequilibration in slowly cooled samples (Lindsley et al. 1991). As the nakhlites are cumulate rocks and therefore subject to slow cooling rates (Mikouchi et al. 2003) it is possible the fO_2 values recorded in the oxides do not reflect crystallization conditions (Treiman and Irving 2008). This is supported by the recognition that the temperatures associated with the oxide fO_2 values are all less than 700 °C (Makishima et al. 2007) and therefore non-magmatic. Conversely, the oxides are known to be late on the liquidus in Martian magmas and the higher fO_2 values may be real and indicative of changing magmatic conditions during crystallization. Determining if these two processes acted alone or in tandem is beyond the scope of this study. The fO_2 estimates based on the qualitative assessment of the pyroxene Eu/Gd ratio (Wadhwa et al. 2004) are consistently higher than those from the Eu-oxybarometer (Fig. 5); however, the qualitative values were determined without the use of a calibrated nakhlite Eu-oxybarometer.

Origin of the fO_2 Range

Unlike terrestrial rocks, recycling through subduction and subsequent convection is not a viable explanation for the range of fO_2 values of the Martian meteorites. However, there are several other processes/mechanisms that may explain the origin of this fO_2 range. These include, but are not limited to, assimilation (e.g., Ague 1998; Parkinson and Arculus 1999), mineral/melt partitioning during partial melting and/or fractional crystallization (e.g., Amundsen and Neumann 1992), shock (e.g., Bauer 1979; Boslough 1991; McCanta et al. 2006), and magma ocean crystallization heterogeneity (e.g., Elkins-Tanton et al. 2003; Borg and Draper 2003). Each will be discussed with respect to Mars below.

Assimilation

Country rock assimilation is known to be both an effective oxidizer (e.g., Parkinson and Arculus 1999; Brandon and Draper 1996; Frost and Ballhaus 1998; Canil et al. 2001) and a potential reducer (Ague 1998; Brenan and Li 2000) depending on the relative oxidation states of the magma and the assimilant. This can lead to changes in the intrinsic fO_2 of a magma on the order of those measured in the Martian meteorites. If assimilation of either solid or liquid material is responsible for these fO_2 variations, one might expect that minerals on the liquidus early would have a different fO_2 than those that crystallize after the assimilation event.

Experimental studies have shown that pyroxenes are one of the first minerals to crystallize from a Martian melt, whereas Fe-Ti oxides come on the liquidus late in the melts crystallization sequence (after 30 and 60% crystallization in hydrous and dry experiments, respectively, to possibly 95% crystallization in the Los Angeles meteorite) (Minitti and Rutherford 2000; Xirouchakis et al. 2002). Therefore pyroxene core fO_2 values should record a different portion of magmatic history than that of the oxides. Earlier work shows that some correlation is observed between the pyroxene and Fe-Ti oxide fO_2 values of the basaltic shergottite class of the Martian meteorites (McCanta et al. 2004). This suggests that the early crystallizing minerals in these meteorites were exposed to the same relative fO_2 environment as the late crystallizing minerals; therefore, this implies that the range of fO_2's of the basaltic shergottites is not caused by assimilation which would have changed the melt fO_2 over the course of crystallization. However, assimilation cannot be completely ruled out on this basis alone. If the assimilation event occurred before any of the existing phenocryst crystallization took place, the primary fO_2 recorded in the phenocrysts would be that of the source region modified by the assimilant.

Unlike the basaltic shergottites (McCanta et al. 2004), the NWA 817 nakhlite shows evidence for an increase in fO_2 of approximately one log unit of relative fO_2 between the earliest crystallized pyroxene phenocrysts and the final groundmass crystallization. In addition, the oxides in the nakhlites, while clearly recording non-magmatic temperature values, may also show some evidence of late-stage oxidation when compared with the pyroxenes (i.e., NWA 817, Nakhla, and NWA 998). Although assimilation may be responsible for local variations in fO_2, this process appears not to be responsible for the whole range of fO_2 values measured in the Martian meteorites.

Mineral/Melt Partitioning

Mineral/melt partitioning (differentiation) can lead to a melt with a higher Fe^{3+}/Fe^{2+} during crystallization of a typical mantle assemblage up to the point when a Fe^{3+}-bearing phase (such as spinel) comes on the liquidus. Early crystallizing minerals generally include olivine and pyroxene, neither of which include significant amounts of Fe^{3+}, thereby causing a buildup of Fe^{3+} and a corresponding increase in the fO_2 of the remaining melt. This increase will be recorded in the crystallizing assemblage. Modeling using the MELTS

program (Ghiorso and Sack 1995) illustrates this process (Fig. 6). MELTS was run at a starting fO_2 of IW+1 based on the results of this study. After obtaining a liquidus temperature, crystallization was begun 10 °C above the liquidus. Equilibrium crystallization was modeled in 10° temperature steps, stopping at 800 °C. For a presumed nakhlite parent melt (NA03 from Stockstill et al., 2005), closed system crystallization at an initial fO_2 of IW+1 increases the Fe^{3+} of the melt by ~49% prior to the onset of spinel crystallization (Fig. 6A). This corresponds to an increase in melt fO_2, calculated using the method of Sack et al. (1980), of 2 orders of magnitude (Fig. 6B). This type of oxidation has been observed in natural terrestrial samples as well. Oxidation of several orders of magnitude has been documented for the Galapagos spreading center through differentiation (Christie et al. 1986; Juster et al. 1989). Similarly, during partial melting Fe^{3+} will again behave incompatibly if one assumes that only olivine and orthopyroxene are left in the melting residue. In this case, Fe^{3+} partitions into the earliest melts, creating melts with higher Fe^{3+} contents and oxidation states than the protolith (Amundsen and Neumann 1992). It is difficult to asses the partial melting process in the nakhlites due to their evolved nature. However, the data suggest that fractionation of a crystallizing, more primitive nakhlite melt could have produced some of the relatively oxidized nakhlites we have sampled.

A potential way to test the differentiation hypothesis is by comparing fO_2 and crystallization sequence. The nakhlites are proposed to have formed through crystallization and accumulation in a thick melt flow or shallow intrusion (e.g., Treiman 2005). If mineral/melt partitioning took place in a cooling lava flow, it is possible that pyroxenes deeper in the cumulate pile may have more reduced fO_2 values than those that crystallized at later times (i.e., shallower depths). Utilizing cooling rates calculated from mineral zoning profiles, Mikouchi et al. (2003) proposed that slower cooling rates were related to deeper burial depths in a single flow or cumulate pile. With this assumption, burial depths of the nakhlites were calculated. Burial depths for the nakhlites from deep to shallow were given as follows: NWA 998, Lafayette, Governador Valadares/Nakhla, Y 593/749, MIL 03346, NWA 817 (Mikouchi et al. 2006). Another option is that the nakhlites did not form in a single flow, but rather in multiple flows (Lentz et al. 2006). Multiple flows have been proposed based on crystal textural characteristics with flow groupings as follows: (NWA 817 {shallow}, Nakhla, Governador Valadares {deep}), (Y 593/749, Lafayette, NWA 998), (MIL 03346). When the calculated fO_2 values in Table 4 are compared to the depth data, a very weak potential correlation between the estimated fO_2 values and depth of crystallization (i.e., time of crystallization) is evident in the single flow projection. If the depth data are accurate, this implies that if differentiation was an important process in the crystallization sequence of the nakhlite magmas, the correlation between fO_2 and crystallization is more complicated than the simple relationship of deep = early crystallizing, shallow = late crystallizing. Alternatively, the depth data for the nakhlites may not be well enough constrained to use as a test for this model.

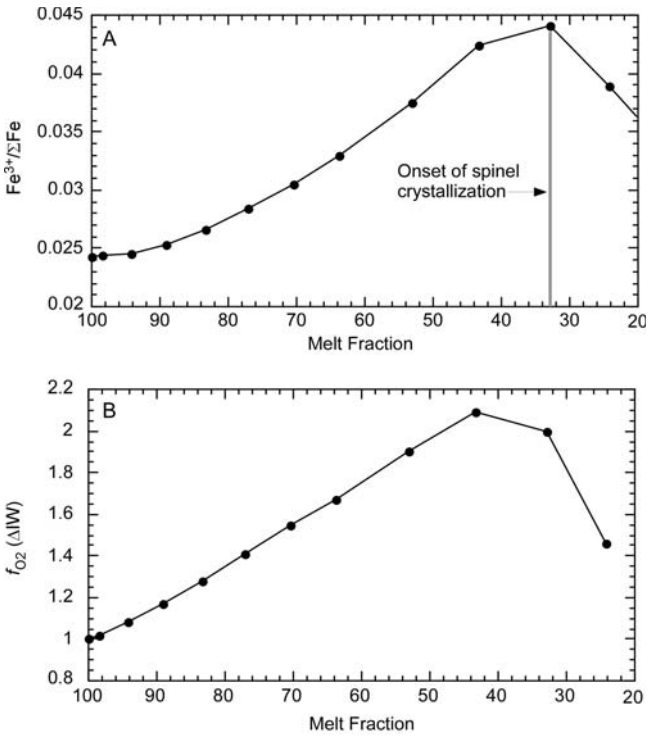

Fig. 6. MELTS calculations of the variation in melt (A) $Fe^{3+}/\Sigma Fe$ and (B) fO_2 for a proposed nakhlite parent melt (NA03 from Stockstill et al. [2005]) during closed system crystallization.

Changes in the melt fO_2 during crystallization can also be investigated by searching for differences in the oxidation state measured in the early crystallizing cores of samples and comparing them to that recorded in the late-stage crystallization products, such as groundmass or FeTi-oxides. Two nakhlites have sufficient remaining groundmass for comparison, MIL 03346 (20%: Day et al. 2006) and NWA 817 (~20%: Sautter et al. 2002). Groundmass analysis is not possible with the other currently recognized nakhlites as they are highly cumulate rocks with little to no groundmass (e.g., Treiman 2005). The fO_2 value estimated from the earliest-crystallizing pyroxene cores in the MIL 03346 and NWA 817 melts are IW+3.2 and IW+2.3, respectively. Both groundmass samples contain the assemblage quartz-fayalite-magnetite indicating that the final crystallization of the samples was near the QFM buffer (IW+3.5). Experiments on a synthetic MIL 03346 composition support this observation and suggest the mesostasis in that meteorite crystallized at IW+4 (Herd and Walton 2008). Within the error bars of the Eu-oxybarometer method, the differences observed in NWA 817 appear to be real and suggest that fO_2 increased approximately one log unit over the course of the crystallization of NWA 817. The fO_2 of MIL 03346 appears to

Table 4. Oxygen fugacity calculations.

	$(Eu/Sm)_{pyx}$[a,b]	$(Eu/Sm)_{melt}$[c]	$D(Eu/Sm)_{pyx/melt}$	fO_2 (ΔIW)
ALH 77005	1.13	1.46	0.77	1.1
LEW 88516	1.05	1.36	0.77	1.1
Y 793605	0.71	1.20	0.59	0.4
Grove Mountain 99027	1.31	1.46	0.90	1.6
MIL 03346	0.82	0.78	1.05	3.2
Nakhla	0.64	0.72	0.88	1.5
Lafayette	0.79	0.80	0.99	2.6
Gov. Valadares	0.81	0.82	0.99	2.6
NWA 998	0.64	0.76	0.84	1.1
NWA 817	0.74	0.77	0.95	2.3
Y 593/749	0.75	0.79	0.95	2.3

[a]Values normalized to chondritic using Anders and Grevasse (1989).

[b]MIL 03346 pyroxene REE values from this study. Pyroxene data for other meteorites is as follows: ALH 77005 (Lundberg et al. 1990); LEW 88516 (Harvey et al. 1993); Y 793605 (Wadhwa et al. 1999); GM 99027 (Hsu et al. 2004); Nakhla, Gov. Valadares, Lafayette (Wadhwa and Crozaz 1995); NWA 998, NWA 817, Y 593.749 (Wadhwa et al. 2004).

[c]Melt REE data for ALH 77005 and MIL 03346 from this study. Melt data for the other meteorites is as follows: LEW 88516 (Dreibus et al. 1992); Y 793605 (Warren and Kallemeyn 1997); GM 99027 (Hsu et al. 2004); Nakhla, Lafayette, Y 593/749 (Dreibus et al. 2003); NWA 817 (Sautter et al. 2002).

have remained relatively constant throughout crystallization, although Rutherford and Hammer (2008) argue that MIL 03346 experienced an fO_2 increase of ~1 log unit over the crystallization period. This difference may result from the error bars associated with the Eu-oxybarometer at the high fO_2 values measured in MIL 03346.

The late crystallizing FeTi-oxides may also provide insight into changing fO_2 conditions as a function of mineral/melt partitioning. The majority of the oxide fO_2 values of Makishima et al. (2007) are higher (relative to the IW buffer) than those recorded in pyroxene using the Eu-oxybarometer (Fig. 5). The differences in calculated fO_2 between the two oxybarometers are between 0.5 and 1.5 log units. These differences are expected if magmatic fO_2 was changing as the result of differentiation. The late crystallizing phase (oxides) would record a different fO_2 than the early crystallizing phase (pyroxene). However, we cannot rule out that the higher fO_2 recorded by the oxides resulted from near-surface oxidation as the magma cooled. The results of all these methods suggest that differentiation is a likely method by which to generate fO_2 variations of ~2 orders of magnitude. This is enough to explain the fO_2 ranges present in the nakhlite suite, but not the four orders of magnitude that both meteorite classes span. Mineral/melt partitioning cannot explain the fO_2 range of the basaltic shergottites for the same reasons given for assimilation, i.e., that the early and late crystallizing minerals record the same fO_2.

Impact-Related Shock

Shock processes are capable of oxidizing (Bauer 1979; Boslough 1991; McCanta et al. 2006) and reducing (Boslough 1991; Beck et al. 2006; Van de Moortèle et al. 2007) the target material they impact into. The effects of shock on mineral composition and oxidation state are not well understood. Olivine in the chassignite NWA 2737 displays nanophase metallic iron indicating a shock reduction episode (Beck et al. 2006; Treiman et al. 2007), resulting from either the shock event itself or the post-shock thermal pulse. Conversely, experimentally shocked clinopyroxenes show large increases in their Fe^{3+}/Fe^{2+} ratios indicating a shock oxidation process (McCanta et al. 2006). The control on whether a shock event produces oxidation or reduction is unclear but, as our knowledge of the oxidation state of Mars is based on meteorites, many of which have been extensively shocked, it is possible that these processes may contribute to the four order of magnitude range in fO_2 values presented above. If shock effects are contributing to the fO_2 range, the most heavily shocked meteorites should have the most extreme oxidized or reduced values. The basaltic shergottites have been subject to shock pressures ranging from 30–40 GPa, the lherzolitic shergottites ~45 GPa, and the nakhlites ~20 GPa (Stöffler 2000). The nakhlites, the least shocked meteorites, are the most heavily oxidized, while the most heavily shocked, the lherzolitic shergottites, are neither highly oxidized nor reduced in comparison to other Martian meteorites (Fig. 4). Although impact-related shock processes may be responsible for small scale variations in measured fO_2 or variations at the local level, they cannot systematically account for the fO_2 range described in this paper.

Incompatible Element Evolution During Magma Ocean Crystallization

As shown above, the Martian meteorites record oxygen fugacities that vary over several orders of magnitude. Variations in fO_2 of <2 orders of magnitude can be produced through processes such as fractionation or assimilation and may be responsible for some of the internal fO_2 variations seen, for example, in some of the nakhlites. However, the complete four log unit range of oxidation states among the Martian meteorite group appears to require an additional explanation. The range of fO_2 values in the Martian

meteorites can be explained through melting of source regions each with a different intrinsic fO_2 value. In this scenario, melts with different fO_2 values are the result of having originated in source regions that are heterogeneous with respect to each other (although they are likely internally homogeneous). The generation of multiple source regions on a body without plate tectonics may be similar to that hypothesized for the lunar interior, which is believed to have produced melts of different compositions from a variety of different source regions, including "normal" basalts and highly enriched KREEP basalts (e.g., Shearer and Papike 1993; Hess and Parmentier 1995). The different magma source regions on the Moon are thought to have formed during crystallization of a lunar magma ocean (e.g., Smith et al. 1970; Wood et al. 1970; Taylor and Jakes 1974; Snyder et al. 1992). The origin of the intrinsic source region differences responsible for the large variation in fO_2 on Mars may also be related to crystallization of a magma ocean early in the planets' history (Herd et al. 2002).

We can investigate the results of Martian magma ocean crystallization, and specifically the role of water during the crystallization process which may aid in producing oxidized regions, through modeling. The crystallization of a Martian magma ocean would proceed in a different fashion than that of the lunar magma ocean due to greater pressures experienced by Martian melts (for a complete discussion of the crystallization process from a petrologic, geochemical, and physical view see: Borg and Draper 2003; Elkins-Tanton et al. 2003) and the potential involvement of volatiles (Elkins-Tanton 2008). Early crystallizing phases would include olivine, two pyroxenes, and garnet (Elkins-Tanton et al. 2003; Borg and Draper 2003). With the exception of garnet, none of the crystallizing minerals take in significant amounts of incompatible elements such as the REEs, Fe^{3+}, or any volatile species. Therefore, this cumulate package represents depleted Martian mantle, a composition comparable in incompatible element composition to terrestrial depleted mantle (i.e., the MORB source [Sun and McDonough 1989]). Melts originating from this region would, among other things, have low initial fO_2 values resulting in rocks with generally low measured fO_2 values.

The addition of a reasonable amount of initial water (0.05 wt%) to the Martian magma ocean does not affect the majority of the crystallization sequence perceptibly. The early crystallizing minerals are all nominally anhydrous, meaning that though they can contain petrologically significant amounts of OH (as much as 1000–1500 ppm for olivine and orthopyroxene) (Koga et al. 2003; Bell et al. 2004; Aubaud et al. 2004; Bolfan-Casanova and Keppler 2000), the effect on the overall water content of the melt is small. It is in the late stages of crystallization that the amount of water becomes significant (Fig. 7A). Continued crystallization of a Martian magma ocean results in build-up of water and other incompatible elements in the remaining liquids, resulting in a highly enriched trapped liquid composition (Borg and Draper 2003) similar to lunar KREEP (e.g., Meyer 1977; Warren and Wasson 1979; Warren 1989). From an initial water content of 0.05 wt%, the remaining melts at >99% crystallization contain 1 wt% water (Elkins-Tanton 2008) (Fig. 7A).

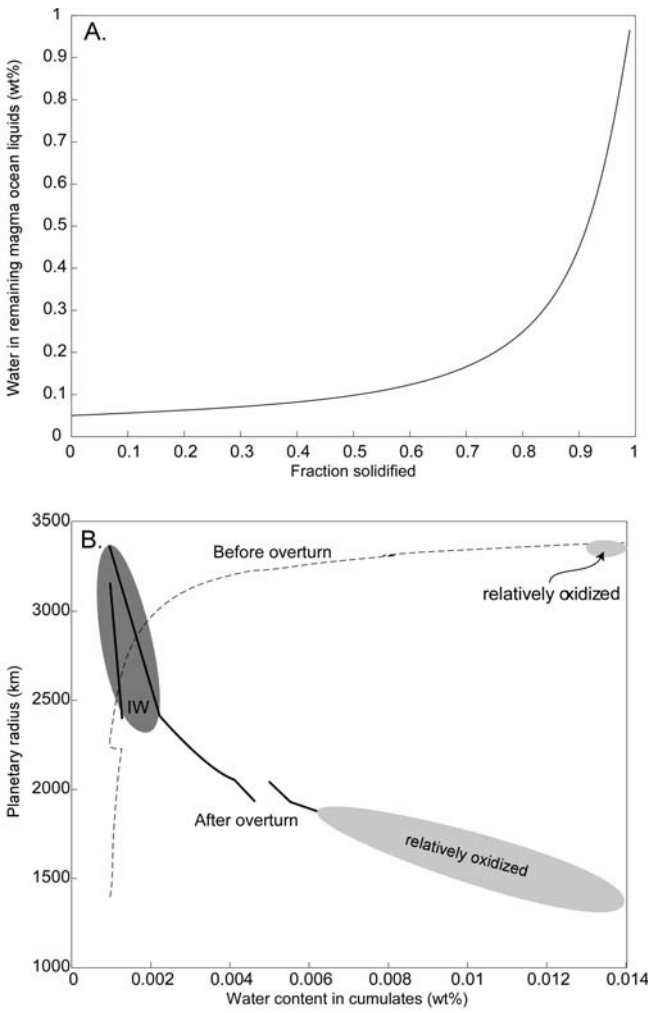

Fig. 7. A) Progressive water enrichment in magma ocean liquids during fractional solidification. By ~90% solidification, remaining magma ocean liquids have obtained ~0.5 wt% of water, if they began with 0.05 wt% water. B) Water content of solidified mantle cumulates. Before overturn to gravitational stability through solid-state flow (dashed line), the most oxidized material is nearest the Martian surface. Following flow to the solid state (bold lines), two regions of lateral heterogeneity are produced in the Martian mantle, and the most oxidized material has mainly sunk to the deep interior, leaving only a small portion frozen in place near the surface. Mantle source regions with oxidation state near IW are delineated with a dark gray oval, and those at higher fO_2s are marked with light gray ovals.

The potential for water to act as an oxidizer is not well constrained. Several studies have linked the presence of water to an increased oxidation state (e.g., Sato and Wright 1966; Baker and Rutherford 1996; Brandon and Draper 1996; Kelley et al. 2007). Other work has suggested that the oxidizing effects of water are insignificant (Moore et al. 1995;

Botcharnikov et al. 2005) or may only be prevalent in somewhat reduced (fO_2 < NNO+1.5 [IW+6]) magmas (Gaillard et al. 2001; Wilke et al. 2002). Although the effect of water addition to a magmatic system is not straightforward, these results suggest that water may have the potential to act as an oxidizing agent in late stage magma ocean melts on Mars. In addition, the buildup in water would be accompanied by a buildup in other incompatible phases as well, such as Fe^{3+}, the REEs, and heat producing elements (i.e., K, U). As described above, increasing crystallization of typical mantle mineral (olivine, pyroxenes) leads to increasing system fO_2 until a ferric-bearing phase begins to crystallize. Therefore, the late-stage crystallization products of the Martian magma ocean should be both hydrous and oxidized. These solids are a potential source region for the most oxidized Martian meteorites.

Models of magma ocean solidification (Elkins-Tanton et al. 2003; Elkins-Tanton et al. 2005; Elkins-Tanton 2008) demonstrate that crystallizing solids in a magma ocean become progressively denser, mainly through iron enrichment, as solidification and liquid evolution proceeds. Solidification therefore results in a cumulate mantle that is unstable to gravitational overturn, and over about one million years flow in the solid state returns the mantle to gravitational stability.

The models used here produce a cumulate mantle with a maximum of about 140 ppm water at the end of solidification, with an oxidation state set during fractional solidification, near the Martian surface (Fig. 7B). These are also the densest cumulates. During overturn in the solid state, some of this highly oxidized material will be too cold and stiff to participate in overturn and will likely remain as a chill crust near the surface, while most will sink to the bottom of the Martian mantle, also carrying with it the bulk of the radiogenic incompatible trace elements (Fig. 7B). Short-lived isotope systematics indicate that this enriched source material must remain separate from the depleted cumulates until melting begins (Jones 1989; Borg et al. 1997; Debaille et al. 2007). The culmination of these processes would result in a Martian mantle heterogeneous with regard to fO_2, among other compositional variables, although single magma source regions may be homogeneous.

Though the presence of trace amounts of water in the final cumulates would decrease their melting temperatures, they retain their cooler surface temperatures as they sink rapidly to depth. There, the combined effects of high pressure and low temperature inhibit melting, while compositional density inhibits convection. Over time, however, the radiogenic enrichment of these late cumulates and heat conducted to them from the core are likely to raise them above their solidi. A partial melt may decrease density sufficiently to produce a rising plume structure, with possible additional melting and eruption. In comparison, the warmer cumulates that rose to nearer the surface during overturn have higher solidi due to both major element composition and water content, but their higher temperature and proximity to the upper boundary make them more likely candidates for early convective adiabatic melting. Thus, both more and less oxidized cumulates may melt and erupt over Martian history.

In this manner magma ocean processes are capable of creating a range of oxidation states similar to those measured in the Martian meteorites and inferred for their source regions. Flow in the solid state to gravitational stability following solidification produces an internal arrangement in which melting source regions of a range of oxidation states are available for later melting. Melting of unoxidized and oxidized reservoirs and percolation and melt reaction can produce the high and low fO_2 end members of the Martian meteorites, and the spectrum of intermediate fO_2 values. A further increase in fO_2 may also occur during partial melting of the late-stage cumulates as the incompatible elements (i.e., Fe^{3+}) would be heavily partitioned into the earliest melts. Additionally, these results may also help explain the known disconnect between the major elements and mineralogy and the incompatible trace elements and fO_2 within these meteorites (e.g., Borg 2002; Herd et al. 2002). In this model, the fO_2 values, as well as the incompatible trace element signatures (Borg 2002; Borg and Draper 2003) are set in the source region as a result of magma ocean crystallization early in Mars history, whereas the major element signatures and mineralogy result from varying degrees of fractional crystallization at a later time, potentially in crustal-level magma chambers (Symes et al. 2008).

CONCLUSIONS

Rehomogenized melt inclusions in the lherzolitic shergottite ALH 77005 and the nakhlite MIL 03346 have been analyzed for their early melt REE compositions. The whole rock REE compositions of these meteorites are observed to be similar in shape to the experimentally determined parent melts, suggesting that whole rock values can be used as proxies for the parent melt in these rocks. This expands the applicability of the Eu-oxybarometer to other nakhlite and lherzolitic shergottite meteorites. The Eu-oxybarometer yields a range of fO_2 values for the lherzolitic shergottites of IW+0.4 to 1.6 and the nakhlites of IW+0.9 to 3.2. When combined with previously calculated fO_2 values for the basaltic shergottites, this results in a range in fO_2 of four orders of magnitude. This is less than the range of terrestrial rocks (nine orders of magnitude), but more than that measured in lunar samples (~one order of magnitude). The origin of this range in fO_2 is not well constrained. Mineral/melt partitioning may result in an fO_2 range of ~2 orders of magnitude. Sampling of different magma source regions, heterogeneous in terms of fO_2, (derived from magma ocean crystallization) provides a method by which a wide range of fO_2 values can be produced. Additional meteorite

finds as well as sample return may clarify the processes that control the fO_2 heterogeneity on Mars.

Acknowledgments—The authors are grateful to the ANSMET program, the NASA Antarctic Meteorite Curator, and the Meteorite Working Group for allowing them access to these meteorites. The assistance of Dr. J. Devine with EMP analysis and Dr. Y. Guan with ion probe analysis was greatly appreciated. Critical reviews by A. Irving, K. Stockstill-Cahill, and A. Treiman helped improve and clarify this work. This research was supported by NASA grant NNG06GF12G to M. J. R. and a Mars Fundamental Research Program grant to L. E. T. A portion of this work was done while M. C. M. was a Urey Post-Doctoral fellow at the Lunar and Planetary Institute.

Editorial Handling—Dr. Allan Treiman

REFERENCES

Ague J. J. 1998. Simple models of coupled fluid infiltration and redox reactions in the crust. *Contributions to Mineralogy and Petrology* 132:180–197.

Amundsen H. E. F. and Neumann E.-R. 1992. Redox control during mantle/melt interaction. *Geochimica et Cosmochimica Acta* 56: 2405–2416.

Anders E. and Grevasse N. 1989. Abundances of the elements: Meteoritic and solar. *Geochimica et Cosmochimica Acta* 53:197–214.

Aubaud C., Hauri E. H., and Hirschmann M. M. 2004. Hydrogen partition coefficients between nominally anhydrous minerals and basaltic melts, *Geophysical Research Letters* 31: doi:10.1029/2004GL021341.

Baker L. L. and Rutherford M. J. 1996. The effect of dissolved water on the oxidation state of silicic melts. *Geochimica et Cosmochimica Acta* 60:2179–2187.

Ballhaus C., Berry R. F., and Green D. H. 1990. Oxygen fugacity controls in the Earth's upper mantle. *Nature* 348:437–440.

Bauer J. F. 1979. Experimental shock metamorphism of mono- and polycrystalline olivine: A comparative study. Proceedings, 10th Lunar and Planetary Science Conference. pp. 2573–2596.

Beck P., Barrat J. A., Gillet Ph., Wadhwa M., Franchi I. A., Greenwood R. C., Bohn M., Cotton J., van de Mootele B., and Reynard B. 2006. Petrography and geochemistry of the chassignite Northwest Africa 2737 (NWA 2737). *Geochimica et Cosmochimica Acta* 70:2127–2139.

Beckett J. R., McCanta M. C., and Stolper E. M. 2008. Phosphorus zoning in SNC olivines (abstract #1391). 39th Lunar and Planetary Science Conference. CD-ROM.

Bell D. R., Rossman G. R., and Moore R. O. 2004. Abundance and partitioning of OH in a high-pressure magmatic system: Megacrysts from the Monastery kimberlite, South Africa. *Journal of Petrology* 45:1539–1564.

Benedix G. K. and Lauretta D. S. 2006. Thermodynamic constraints on the formation of the acapulcoites (abstract #2129). 37th Lunar and Planetary Science Conference. CD-ROM.

Bischoff A., Geiger T., Palme H., Spettel B., Schultz L., Scherer P., Loeken T., Bland P., Clayton R. N., Mayeda T. K., Herpers U., Meltzow B., Michel R., and Dittrich-Hannen B. 1994. Acfer 217—a new member of the Rumuruti chondrite group (R). *Meteoritics* 29:264–274.

Blinova A. and Herd C. D. K. 2008. Experimental partitioning of REE using a primitive Martian basalt composition. *Geochimica et Cosmochimica Acta* 72:A90.

Bolfan-Casanova N. and Keppler H. 2000. Water partitioning between nominally anhydrous minerals in the MgO-SiO_2-H_2O system up to 24 GPa: implications for the distribution of water in the Earth's mantle. *Earth and Planetary Science Letters* 182: 209–221.

Borg L. E., Nyquist L. E., Taylor L. A., Wiesmann H., and Shih C.-Y. 1997. Constraints on Martian differentiation processes from Rb-Sr and Sm-Nd isotopic analyses of the basaltic shergottite QUE 94201. *Geochimica et Cosmochimica Acta* 61:4915–4931.

Borg L. E. 2002. Exploring trace element and isotopic mixing relationships in the Martian meteorite suite (abstract #6004). Workshop on Unmixing the SNCs.

Borg L. E. and Draper D. S. 2003. A petrogenetic model for the origin and compositional variation of the Martian basaltic meteorites. *Meteoritics & Planetary Science* 38:1713–1732.

Boslough M. B. 1991. Shock modification and chemistry and planetary geologic processes. *Annual Review of Earth and Planetary Science* 19:1010–130.

Botcharnikov R. E., Koepke J., Holtz F., McCammon C., and Wilke M. 2005. The effect of water activity on the oxidation and structural state of Fe in a ferro-basaltic melt. *Geochimica et Cosmochimica Acta* 69:5071–5085.

Brandon A. D. and Draper D. S. 1996. Constraints on the origin of the oxidation state of mantle overlying subduction zones: An example from Simcoe, Washington, USA. *Geochimica et Cosmochimica Acta* 60:1739–1749.

Brearley A. J. and Jones R. H. 1998. Chondritic meteorites. In *Planetary materials*, edited by J. J. Papike. Reviews in Mineralogy, vol. 36, Washington, D.C.: Mineralogical Society of America.

Brenan J. M. and Li C. 2000. Constraints on oxygen fugacity during sulfide segregation in the Voisey's Bay intrusion, Labrador, Canada. *Economic Geology* 95:901–915.

Brett R. 1984. Chemical equilibration of the Earth's core and upper mantle. *Geochimica et Cosmochimica Acta* 48:1183–1188.

Buddington A. F. and Lindsley D. H. 1964. Iron-titanium oxide minerals and synthetic equivalents. *Journal of Petrology* 5:310–357.

Calvin C. and Rutherford M. J. 2008. The parental melt of lherzolitic shergottite ALH 77005: A study of rehomogenized melt inclusions. *American Mineralogist* 93:1886–1898.

Canil D., O'Neill H. St. C., Pearson D. G., Rudnick R. L., McDonough W. F., and Carswell D. A. 2001. Ferric iron in peridotites and mantle oxidation states. *Earth and Planetary Science Letters* 123:205–220.

Carmichael I. S. E. 1991. The oxidation state of basic magmas: A reflection of their source region? *Contributions to Mineralogy and Petrology* 106:129–142.

Chabot N. L. and Agee C. B. 2003. Core formation in the Earth and Moon: New experimental constraints from V, Cr, and Mn. *Geochimica et Cosmochimica Acta* 67:2077–2091.

Cherniak D. J. 2001. Pb diffusion in Cr diopside, augite, and enstatite, and consideration of the dependence of cation diffusion in pyroxene on oxygen fugacity. *Chemical Geology* 177:381–397.

Christie D. M. and J. M. Sinton 1986. Major element constraints on melting, differentiation and mixing of magmas from the Galapagos 95.5°W propagating rift system *Contributions to Mineralogy and Petrology* 94:274–288.

Cottrell E., Spiegelman M., and Langmuir C. H. 2002. Consequences of diffusive reequilibration for the interpretation of melt inclusions. *Geochemistry Geophysics Geosystems* 3, doi:10.1029/2001GC000205.

Cottrell E. and Walker D. 2006. Constraints on core formation from

Pt partitioning in mafic silicate liquids at high temperatures. *Geochimica et Cosmochimica Acta* 70:1565–1580.

Dann J. C., Holzheid A. H., Grove T. L., and McSween H. Y. Jr. 2001. Phase equilibria of the Shergotty meteorite: Constraints on pre-eruptive water contents of martian magmas and fractional crystallization under hydrous conditions. *Meteoritics & Planetary Science* 36:793–806.

Danyushevsky L. V., McNeill A. W., and Sobolev A. V. 2002. Experimental and petrological studies of melt inclusions in phenocrysts from mantle-derived magmas: An overview of techniques, advantages and complications. *Chemical Geology* 183:5–24.

Day J. M., Taylor L. A., Floss C., and McSween H. Y. Jr. 2006. Petrology and chemistry of MIL 03346 and its significance in understanding. The petrogenesis of nakhlites on Mars. *Meteoritics* 41:581–606.

Debaille V., Brandon A. D., Yin Q. Z., and Jacobsen B. 2007. Coupled ^{142}Nd–^{143}Nd evidence for a protracted magma ocean in Mars. *Nature* 450:525–528.

Domeneghetti M. C., Fioretti A. M., Camara F., Molin G., and McCammon C. 2006. Constraints on the thermal history and oxidation state of MIL 03346 Martian meteorite: Single-crystal XRD, electron microprobe and Mössbauer analyses of clinopyroxene (abstract #1238). 37th Lunar and Planetary Science Conference. CD-ROM.

Dreibus G., Jochum K. H., Palme H., Spettel B., Wlotzka F., and Wänke H. 1992. LEW 88516: A meteorite compositionally close to the "Martian mantle" (abstract). *Meteoritics* 27:216–217.

Dreibus G., Huisl W., Spettel B., and Haubold R. 2003. Comparison of the chemistry of Y-000593 and Y-000749 with other nakhlites (abstract #1586). 34th Lunar and Planetary Science Conference. CD-ROM.

Edmunson J., Borg L. E., Shearer C. K., and Papike J. J. 2005. Defining the mechanisms that disturb the Sm-Nd isotopic systematics of the Martian meteorites: Examples from Dar al Gani 476 and Allan Hills 77005. *Meteoritics & Planetary Science* 40:1159–1174.

Elkins-Tanton L. T., Parmentier E. M., Hess P. C. 2003. Magma ocean fractional crystallization and cumulate overturn in terrestrial planets: Implications for Mars. *Meteoritics & Planetary Science* 38:1753–1771.

Elkins-Tanton L. T., Parmentier E. M., and Hess P. C. 2005. The formation of ancient crust on Mars through magma ocean processes. *Journal of Geophysical Research* 110: doi:10.1029/2005JE002480.

Elkins-Tanton L. T. 2008. Linked magma ocean solidification and atmospheric growth for Earth and Mars. *Earth and Planetary Science Letters* 71:181–191.

Frost B. R. and Ballhaus C. 1998. Comment on "Constraints on the origin of the oxidation state of mantle overlying subduction zones: An example from Simcoe, Washington, USA." *Geochimica et Cosmochimica Acta* 62:329–331.

Gaetani G. A. and Watson E. B. 2000. Open system behavior of olivine-hosted melt inclusions. *Earth and Planetary Science Letters* 183:27–41.

Gaillard F., Scaillet B., Pichavant M., and Bény J-M. 2001. The effect of water and fO_2 on the ferric–ferrous ratio of silicic melts. *Chemical Geology* 174:255–273.

Ghiorso M. S. and Sack R. O. 1995. Chemical mass transfer in magmatic processes. IV. A revised and internally consistent thermodynamic model for the interpolation and extrapolation of liquid-solid equilibria in magmatic systems at elevated temperatures and pressures. *Contributions to Mineralogy and Petrology* 119:197–212.

Ghosal S., Sack R. O., Ghiorso M. S., and Lipschutz M. E. 1998. Evidence for a reduced, Fe-depleted Martian mantle source region of shergottites. *Contributions to Mineralogy and Petrology* 130:346–357.

Goodrich C. A., Herd C. D. K., and Taylor L. A. 2003. Spinels and oxygen fugacity in olivine-phyric and lherzolitic shergottites. *Meteoritics & Planetary Science* 38: 1773–1792.

Goodrich C. A. and Harvey R. P. 2002. The parent magmas of lherzolitic shergottites ALH 77005 and LEW 88516: A reevaluation from magmatic inclusions in olivine and chromite (abstract# 5123). *Meteoritics & Planetary Science*.

Haggerty S. E. 1978. The redox state of planetary basalts. *Geophysical Research Letters* 5:443–446.

Hammer J. E. and Rutherford M. J. 2005. Experimental crystallization of Fe-rich basalt: Application to cooling rate and oxygen fugacity of nakhlite MIL 03346 (abstract #1999). 36th Lunar and Planetary Science Conference. CD-ROM.

Harvey R. P., Wadhwa M., McSween Jr. H. Y., and Crozaz G. 1993. Petrography, mineral chemistry, and petrogenesis of Antarctic shergottite LEW 88516. *Geochimica et Cosmochimica Acta* 57: 4769–4783.

Herd C. D. K., Papike J. J., and Brearley A. J. 2001. Oxygen fugacity of Martian basalts from electron microprobe oxygen and TEM-EELS analyses of Fe-Ti oxides. *American Mineralogist* 86: 1015–1024.

Herd C. D. K., Borg L. E., Jones J. H., and Papike J. J. 2002. Oxygen fugacity and geochemical variations in the Martian basalts: Implications for martian basalt petrogenesis and the oxidation state of the upper mantle of Mars. *Geochimica et Cosmochimica Acta* 66:2025–2036.

Herd C. D. K. 2003. The oxygen fugacity of olivine-phyric Martian basalts and the components within the mantle and crust of Mars. *Meteoritics & Planetary Science* 38:1793–1805.

Herd C. D. K. and Walton E. L. 2008. Cooling and crystallization of the Miller Range 03346 nakhlite: Insights from experimental petrology and mineral equilibria (abstract #1496). 39th Lunar and Planetary Science Conference. CD-ROM.

Hess P. C. and Parmentier E. M. 1995. A model for the thermal and chemical evolution of the Moon's interior: Implications for the onset of mare volcanism. *Earth and Planetary Science Letters* 134:501–514.

Hsu W., Guan Y., Wang H., Leshin L. A., Wang R., Zhang W., Chen X., Zhang F., and L in C. 2004. The lherzolitic shergottite Grove Mountain 99027: Rare earth element geochemistry. *Meteoritics & Planetary Science* 39:701–709.

Ikeda Y. 1994. Petrography and petrology of ALH 77005 shergottite. *Proceedings of the NIPR Symposium on Antarctic Meteorites* 7: 9–29.

Ikeda Y. 1998. Petrology of magmatic silicate inclusions in the ALH 77005 lherzolitic shergottite. *Meteoritics & Planetary Science* 33:803–812.

Imae N. and Ikeda Y. 2007. Petrology of the Miller Range 03346 nakhlite in comparison with the Yamato-000593 nakhlite. *Meteoritics & Planetary Science* 42:171–184.

Johnson M. C., Rutherford M. J., and Hess P. C. 1991. Chassigny petrogenesis: Melt composition, intensive parameters, and water contents of Martian (?) magmas. *Geochimica et Cosmochimica Acta* 55:349–366.

Jones J. H. 1989. Isotopic relationships among the shergottites, the nakhlites and chassigny. Proceedings, 19th Lunar and Planetary Science Conference. pp. 465–474.

Juster T. C., Grove T. L., and Perfit M. R. 1989. Experimental constraints on the generation of FeTi basalts, andesites, and rhyodacites at the Galapagos Spreading Center 85°W and 95°W. *Journal of Geophysical Research* 94:9251–9274.

Kallemeyn G. W., Rubin A. E., and Wasson J. T. 1996. The compositional classification of chondrites: VII. The R chondrite group. *Geochimica et Cosmochimica Acta* 60:2243–2256.

Karner J. M., Sutton S. R., Papike J. J., Shearer C. K., Jones J. H., and Newville M. 2006. Application of a new vanadium valence oxybarometer to basaltic glasses from the Earth, Moon, and Mars. *American Mineralogist* 91:270–277.

Karner J. M., Papike J. J., Sutton S. R., Shearer C. K., McKay G., Le L., and Burger P. 2007a. Valence state partitioning of Cr between pyroxene-melt; effects of pyroxene and melt composition and direct determination of Cr valence states by XANES; application to Martian basalt QUE 94201 composition. *American Mineralogist* 92:2002–2005.

Karner J. M., Papike J. J., Shearer C. K., McKay G., Le L., and Burger P. 2007b. Valence state partitioning of Cr and V between pyroxene-melt; estimates of oxygen fugacity for Martian basalt QUE 94201. *American Mineralogist* 92:1238–1241.

Kelley K. A., Cottrell E., Fischer R. 2007. Water and the oxidation state of global arc and MORB magmas (abstract). *EOS* 88, Fall Meeting Supplement.

Koga K., Hauri E., Hirschmann M., and Bell D. 2003. Hydrogen concentration analysis using SIMS and FTIR: Comparison and calibration for nominally anhydrous minerals. *Geochemistry Geophysics Geosystems* 4, doi:10.1029/2002GC000378.

Kress V. and Carmichael I. S. E. 1991. The compressibility of silicate liquids containing Fe_2O_3 and the effect of composition, temperature, oxygen fugacity, and pressure on their redox states. *Contributions to Mineralogy and Petrology* 108:82–92.

Langenhorst F., Stöffler D., and Klein D. 1991. Shock metamorphism of the Zagami achondrite (abstract). 22nd Lunar and Planetary Science Conference. pp. 779–780.

Larimer J. W. and Wasson J. T. 1988. Siderophile element fractionation. In *Meteorites and the early solar system*, edited by Kerridge J. F. and Matthews M. S. Tucson, Arizona: The University of Arizona Press. pp. 416–435.

Lentz R. C. F., McCoy T. J., and Taylor G. J. 2006. Multiple nakhlite lava flows? (abstract). *Meteoritics & Planetary Science* 40:A91.

Li J. and Agee C. B. 2001. The effect of pressure, temperature, oxygen fugacity and composition on partitioning of nickel and cobalt between liquid Fe-Ni-S alloy and liquid silicate: Implications for the Earth's core formation. *Geochimica et Cosmochimica Acta* 65:1821–1832.

Lindsley D. H., Frost B. R., Ghiorso M. S., and Sack R. O. 1991. Oxides lie; the Bishop Tuff did not erupt from a thermally zoned magma body (abstract). *EOS* 72:312.

Lodders K. 1998. A survey of shergottite, nakhlite, and Chassigny meteorite whole rock compositions. *Meteoritics & Planetary Science* 33:A183–190.

Longhi J. and Pan V. 1989. The parent magmas of the SNC meteorites. Proceedings, 19th Lunar and Planetary Science Conference. pp. 451–464.

Lundberg L. L., Crozaz G., McKay G., and Zinner E. 1988. Rare earth element carriers in the Shergotty meteorite and implications for its chronology. *Geochimica et Cosmochimica Acta* 52:2147–2163.

Lundberg L. L., Crozaz G., and McSween Jr. H. Y. 1990. Rare earth elements in minerals of the ALH 77005 shergottite and implications for its parent magma and crystallization history. *Geochimica et Cosmochimica Acta* 54:2535–2547.

Lundstrom C. C., Shaw H. F., Ryerson F. J., Williams Q., and Gill J. 1998. Crystal chemical control of clinopyroxene-melt partitioning in the Di-Ab-An system; implications for elemental fractionations in the depleted mantle. *Geochimica et Cosmochimica Acta* 62:2849–2862.

Ma M.-S., Laul J. C., and Schmitt R. A. 1981. Complementary rare earth element patterns in unique achondrites, such as ALHA77005 and shergottites, and in the earth. Proceedings, 12th Lunar and Planetary Science Conference, part B. pp. 1349–1358.

Makishima J., McKay G., Le L., Miyamoto M., and Mikouchi T. 2006. Calibration of the Eu oxybarometer for nakhlites (abstract #1589). 37th Lunar and Planetary Science Conference. CD-ROM.

Makishima J., McKay G., Le L., Miyamoto M., and Mikouchi T. 2007. Oxidation state of nakhlites as inferred from Fe-Ti oxide equilibria and augite/melt europium partitioning (abstract #1834). 38th Lunar and Planetary Science Conference. CD-ROM.

McCanta M. C., Rutherford M. J., and Jones J. H. 2004. An experimental study of rare earth element partitioning between a shergottite melt and pigeonite: Implications for the oxygen fugacity of the martian interior. *Geochimica et Cosmochimica Acta* 68:1943–1952.

McCanta M. C., Dyar M. D., and Hörz F. 2006. Shock oxidation of pyroxene: Effects on redox ratio (abstract #1903). 37th Lunar and Planetary Science Conference. CD-ROM.

McCoy T. J., Taylor G. J., and Keil K. 1992. Zagami: Product of a two-stage magmatic history. *Geochimica et Cosmochimica Acta* 56:3571–3582.

McKay G., Le L., Wagstaff J., and Crozaz G. 1994. Experimental partitioning of rare earth elements and strontium: Constraints on petrogenesis and redox conditions during crystallization of Antarctic angrite Lewis Cliff 86010. *Geochimica et Cosmochimica Acta* 58:2911–2919.

McSween H. Y. Jr., Taylor L. A., and Stolper E. M. 1979. Allan Hills 77005: A new meteorite type found in Antarctica. *Science* 204: 1201–1203.

McSween H. Y. Jr. 1994. What we have learned about Mars from SNC meteorites. *Meteoritics* 29:757–779.

McSween H. Y. Jr., Eisenhour D. D., Taylor L. A., Wadhwa M., and Crozaz G. 1996. QUE 94201 shergottite: Crystallization of a Martian basaltic magma. *Geochimica et Cosmochimica Acta* 60: 4563–4569.

Meyer C. Jr. 1977. Petrology, mineralogy, and chemistry of KREEP basalt. *Physics, Chemistry and Earth Sciences* 10:239–260.

Mikouchi T. and Miyamoto M. 2000. Lherzolitic Martian meteorites Allan Hills 77005, Lewis Cliff 88516 and Yamato-793605: Major and minor element zoning in pyroxene and plagioclase glass. *Antarctic Meteorite Research* 13:256–269.

Mikouchi T., Koizumi E., Monkawa A., Ueda Y., and Miyamoto M. 2003. Mineralogy and petrology of Yamato 000593: Comparison with other Martian nakhlite meteorites. *Antarctic Meteorite Research* 16:34–57.

Mikouchi T., Miyamoto M., Koizumi E., Makishima J., and McKay G. 2006. Relative burial depths of nakhlites: An update (abstract #1865). 37th Lunar and Planetary Science Conference. CD-ROM.

Milman-Barris M. S., Beckett J. R., Baker M. B., Hoffman A. E., Morgan Z., Crowley M. R., Vielzeuf D., and Stolper E. M. 2008. Zoning of phosphorus in igneous olivine. *Contributions to Mineralogy and Petrology* 155:739–765.

Minitti M. E. and Rutherford M. J. 2000. Genesis of the Mars Pathfinder "sulfur-free" rock from SNC parental liquids. *Geochimica et Cosmochimica Acta* 64:2535–2547.

Moore G., Righter K., and Carmichael I. S. E. 1995. The effect of dissolved water on the oxidation state of iron in natural silicate liquids. *Contributions to Mineralogy and Petrology* 120:170–179.

Musselwhite D. S. and Jones J. H. 2003. Oxygen fugacity of the Martian mantle from pyroxene/melt partitioning of REE (abstract# 2032). 34th Lunar and Planetary Science Conference. CD-ROM.

Nakamura T., Tomeoka K., and Takeda H. 1993. Mineralogy and petrology of the CK chondrites Yamato-82104, -693 and a

Carlisle Lakes-type chondrite Yamato-82002. *Proceedings of the NIPR Symposium on Antarctic Meteorites* 6:171–185.

Nicholis M. G. and Rutherford M. J. 2005. Pressure dependence of graphite-C-O phase equilibria and its role in lunar mare volcanism (abstract #1726). 36th Lunar and Planetary Science Conference. CD-ROM.

O'Neill H. St. C. and Wall V. J. 1987. The olivine-orthopyroxene-spinel oxygen geobarometer, the nickel precipitation curve, and the oxygen fugacity of the Earth's upper mantle. *Journal of Petrology* 28:1169–1191.

O'Neill H. St. C. 2004. Oxygen and core formation in the earth (abstract #3018). Workshop on Oxygen in the Terrestrial Planets.

Palme H. and O'Neill H. St. C. 1996. Formation of the Earth's core. *Geochimica et Cosmochimica Acta* 60:1106–1108.

Parkinson I. J. and Arculus R. J. 1999. The redox state of subduction zones: Insights from arc peridotites. *Chemical Geology* 160:409–423.

Righter K. and Drake M. J. 1996. Core formation in Earth's moon, Mars, and Vesta. *Icarus* 124:513–529.

Roeder P. L. 1974. Activity of iron and olivine solubility in basaltic liquids. *Earth and Planetary Science Letters* 23:397–410.

Rubin A. E. and Kallemeyn G. W. 1994. Pecora Escarpment 91002: A member of the new Rumuruti (R) chondrite group. *Meteoritics* 29:255–264.

Rutherford M. J., Calvin C., Nicholis M., McCanta M. C. 2005. Petrology and melt compositions in nakhlite MIL-03346: Significance of data from natural sample and from experimentally fused groundmass and M.I.'s (abstract #2233). 36th Lunar and Planetary Science Conference. CD-ROM.

Rutherford M. J. and Hammer J. E. 2008. Oxidation states in MIL 03346 nakhlite from experiments reproducing phenocryst-melt equilibria as a function of fO_2 and T at 40–150 MPa (abstract #1983). 39th Lunar and Planetary Science Conference. CD-ROM.

Sack R. O., Carmichael I. S. E., Rivers M., and Ghiorso M. S. 1980. Ferric-ferrous equilibria in natural silicate liquids at 1 bar. *Contributions to Mineralogy and Petrology* 75:369–376.

Sato M., Hickling N. L., and McLane J. E. 1973. Oxygen fugacity values of Apollo 12, 14, and 15 lunar samples and reduced state of lunar magmas. Proceedings, 4th Lunar Science Conference. pp. 1061–1079.

Sato M. 1978. Oxygen fugacity of basaltic magmas and the role of gas forming elements. *Geophysical Research Letters* 5:447–449.

Sato M. and Wright T. L. 1966. Oxygen fugacities directly measured in magmatic gases. *Science* 153:1103–1105.

Sautter V., Barrat J. A., Jambon A., Lorand J. P., Gillet Ph., Javoy M., Joron J. L., and Lesourd M. 2002. A new Martian meteorite from Morocco: The nakhlite Northwest Africa 817. *Earth and Planetary Science Letters* 195:223–238.

Schulze H., Bischoff A., Palme H., Spettel B., Dreibus G., and Otto J. 1994. Mineralogy and chemistry of Rumuruti: The first meteorite fall of the new R-chondrite group. *Meteoritics* 29:275–286.

Schwandt C. S. and McKay G. A. 1998. Rare earth element partition coefficients from enstatite/melt synthesis experiments. *Geochimica et Cosmochimica Acta* 62:2845–2848.

Shearer C. K. and Papike J. J. 1993. Basaltic volcanism on the Moon: A perspective from volcanic picritic glass beads. *Geochimica et Cosmochimica Acta* 57:4785–4812.

Shearer C. K., McKay G., Papike J. J., and Karner J. M. 2006. Valence state partitioning of vanadium between olivine-liquid; estimates of the oxygen fugacity of Y980459 and application to other olivine-phyric Martian basalts. *American Mineralogist* 91: 1657–1663.

Smith J. V., Anderson A. T., Newton R. C., Olsen E. J., Wyllie P. J., Crewe A. V., Isaacson M. S., and Johnson D. 1970. Petrologic history of the moon inferred from petrography, mineralogy, and petrogenesis of Apollo 11 rocks. *Proceedings of the Apollo 11 Lunar Science Conference.* pp. 897–925.

Smith M. R., Laul J. C., Ma M. S., Huston T., Verkouteren R. M., Lipschutz M. E., and Schmitt R. A. 1984. Petrogenesis of the SNC (shergottites, nakhlites, chassignites) meteorites: Implications for their origin from a large dynamic planet, possibly Mars. Proceedings, 14th Lunar and Planetary Science Conference. *Journal of Geophysical Research* 89:B612–B630.

Snyder G. A., Taylor L. A., and Neal C. R. 1992. A chemical model for generating the sources of mare basalts: Combined equilibrium and fractional crystallization of the lunar magmasphere. *Geochimica et Cosmochimica Acta* 56:3809–3823.

Stockstill K. R., McSween H. Y. Jr., and Bodnar R. J. 2005. Melt inclusions in augite of the Nakhla martian meteorite: Evidence for basaltic parental melt. *Meteoritics & Planetary Science* 40: 377–396.

Stöffler D., Ostertag R., Jammes C., Pfannschmidt G., Sen Gupta P. R., Simon S. B., Papike J. J., and Beauchamp R. H. 1986. Shock metamorphism and petrography of the Shergotty achondrite. *Geochimica et Cosmochimica Acta* 50:889–913.

Stöffler D. 2000. Maskelynite confirmed as diaplectic glass: indication for peak shock pressures below 45 GPa in all Martian meteorites (abstract #1170). 31st Lunar and Planetary Science Conference.

Stolper E. and McSween Jr. H. Y. 1979. Petrology and origin of the shergottite meteorites. *Geochimica et Cosmochimica Acta* 43: 1475–1498.

Stolper E. 1977. Experimental petrology of eucritic meteorites. *Geochimica et Cosmochimica Acta* 41:587–611.

Sun S.-S. and McDonough W. F. 1989. Chemical and isotopic systematics of oceanic basalts: Implications for mantle composition and processes. In *Magmatism in the ocean basins*, Saunders, A. D. and Norry M. J. Geological Society of London Special Publication 42.

Symes S. J. K., Borg L. E., Shearer C. K., and Irving A. J. 2008. The age of the Martian meteorite Northwest Africa 1195 and the differentiation history of the shergottites. *Geochimica et Cosmochimica Acta* 72:1696–1710.

Taylor S. R. and Jakes P. 1974. The geochemical evolution of the moon. Proceedings, 5th Lunar Science Conference. pp. 1287–1305.

Treiman A. H. 1996. The perils of partition: Difficulties in retrieving magma compositions from chemically equilibrated basaltic meteorites. *Geochimica et Cosmochimica Acta* 60:147–155.

Treiman A. H. 2005. The nakhlite meteorites: Augite-rich igneous rocks from Mars. *Chemie der Erde* 65:203–270.

Treiman A. H., Dyar M. D., McCanta M., Pieters C. M., Hiroi T., Lane M. D., and Bishop J. 2007. Martian dunite NWA 2737: Petrographic constraints geological history, shock events, and olivine color. *Journal of Geophysical Research* 112: E04002, doi:10.1029/2006JE002777.

Treiman A. H. and Irving A. J. 2008. Petrology of Martian meteorite Northwest Africa 998. *Meteoritics & Planetary Science* 43:829–854.

Van de Moortèle B., Reynard B., McMillan P. F., Wilson M., Beck P., Gillet P., and Jahn S. 2007. Shock-induced transformation of olivine to a new metastable $(Mg,Fe)_2SiO_4$ polymorph in Martian meteorites. *Earth and Planetary Science Letters* 261:469–475.

Van Orman J. A., Grove T. L., and Shimizu N. 2001. Rare earth element diffusion in diopside: Influence of temperature, pressure, and ionic radius, and an elastic model for diffusion in silicates. *Contributions to Mineralogy and Petrology* 141:687–703.

Varela M. E., Kurat G., and Clocchiatti R. 2001. Glass-bearing

inclusions in Nakhla (SNC meteorite) augite: Heterogeneously trapped phases. *Mineralogy and Petrology* 71:155–172.

Usselman T. M. and Lofgren G. E. 1976. The phase relations, textures, and mineral chemistries of high titanium mare basalts as a function of oxygen fugacity and cooling rate. Proceedings, 7th Lunar Science Conference. pp. 1345–1363.

Wadhwa M., McSween Jr. H. Y., and Crozaz G. 1994. Petrogenesis of shergottite meteorites inferred from minor and trace element microdistribution. *Geochimica et Cosmochimica Acta* 58:4213–4229.

Wadhwa M. and Crozaz G. 1995. Trace and minor elements of nakhlites and Chassigny: Clues to their petrogenesis. *Geochimica et Cosmochimica Acta* 59:3629–3645.

Wadhwa M., McKay G. A., and Crozaz G. 1999. Trace element distributions in Yamato 793605, a chip off the "Martian lherzolite" block. *Antarctic Meteorite Research* 12:168–182.

Wadhwa M. 2001. Redox state of Mars' upper mantle and crust from Eu anomalies in shergottite pyroxenes. *Science* 291:1527–1530.

Wadhwa M., Crozaz G., and Barrat J-A. 2004. Trace element distributions in the Yamato 000593/000749, NWA 817, and NWA 998 nakhlites: Implications for their petrogenesis and mantle source on Mars. *Antarctic Meteorite Research* 17:97–116.

Walker D. and Grove T. 1993. Ureilite smelting. *Meteoritics* 28:629–636.

Wänke H., Dreibus G., Jagoutz E., Palme H., Spettel B., and Weckwerth G. 1986. ALHA77005 and on the chemistry of the Shergotty parent body (Mars) (abstract). 17th Lunar and Planetary Science Conference. pp. 919–920.

Warren P. H. and Wasson J. T. 1979. The origin of KREEP. *Reviews of Geophysics and Space Physics* 17:73–88.

Warren P. H. 1989. KREEP: Major-element diversity, trace element uniformity (almost). In *Workshop on Moon in Transition: Apollo 14, KREEP, and Evolved Lunar Rocks*, LPI Technical Report 89-03:149–153.

Warren P. H. and Kallemeyn G. W. 1997. Yamato-793605, EET 79001, and other presumed Martian meteorites: Compositional clues to their origins. *Antarctic Meteorite Research* 10:61–81.

Wilke M., Behrens H., Burkhard D. J. M., and Rossano S. 2002. The oxidation state of iron in silicic melt at 500 MPa water pressure. *Chemical Geology* 189:55–67.

Wood B. J. 1991. Oxygen barometry of spinel peridotites. In *Oxide minerals: Petrologic and magmatic significance*, edited by Lindsley D. H. Chantilly, Virginia: Reviews in Mineralogy, vol. 25. Mineralogical Society of America. pp. 417–431.

Wood J. A., Dickey J. S., Marvin U. B., and Powell B. N. 1970. Lunar anorthosites and a geophysical model of the moon. *Proceeding of the Apollo 11 Lunar Science Conference*. pp. 965–988.

Xirouchakis D., Draper D. S., Schwandt C. S., and Lanzirotti, A. 2002. Crystallization conditions of Los Angeles, a basaltic Martian meteorite. *Geochimica et Cosmochimica Acta* 66:1867–1880.

Zinner E. and Crozaz G. 1986. A method for the quantitative measurement of rare earth elements in the ion microprobe. *International Journal of Mass Spectrometry and Ion Processes* 69:17–38.

Zipfel J. and Goodrich C. A. 2001. REE in melt inclusions in olivine of ALHA77005 (abstract #5192). 54th Annual Meeting of the Meteoritical Society. *Meteoritics & Planetary Science* 36.